Materials Today Communications 56 (2026) 115963

Contents lists available at ScienceDirect

Materials Today Communications

journal homepage: www.elsevier.com/locate/mtcomm

A multi-stable metamaterial design method (MSMDM) based on a bistable chiral structure

Pierre Roberjot [a,*], Jonathan B. Hopkins [b], Just L. Herder [a]

[a] Delft University of Technology, Department of Precision and Microsystems Engineering, Mekelweg 2, Delft 2628CD, the Netherlands
[b] University of California Los Angeles, Department of Mechanical and Aerospace Engineering, 420 Westwood Plaza, Los Angeles, CA 90095, USA

ARTICLE INFO

Keywords:
Metamaterials
Multistability
Bistability
Rational design
Snap-through

ABSTRACT

The design of multistable metamaterials has predominantly relied on trial-and-error strategies and geometry-specific optimization, limiting systematic exploration of design spaces. Despite numerous reported architectures, unified approaches for the generation and classification of planar and spatial multistable systems remain underdeveloped. This work introduces the Multistable Metamaterial Design Method (MSMDM), a topology-driven generative framework for the systematic discovery, classification, and nomenclature of multistable structures. Starting from a fundamental chiral bistable seed (Z_B) and its spatial extension (Z_{3B}), the method employs a discrete set of seven topological transformations to reconstruct existing designs and generate new multistable families. A key contribution is the definition of the superchirality order χ, a compact descriptor that enables consistent characterization of chirality across dimensions and captures its evolution during structural transformations. The MSMDM is demonstrated to reproduce structures that exhibit a broad spectrum of mechanical responses, including monostable, neutrally stable, and countersnapping behaviors exhibiting contraction under extension. By defining unit cells through a Voronoi-based formalism, the framework ensures compatibility with scalable planar and spatial tessellations. Overall, MSMDM establishes a unified design language that decouples topological generation from mechanical optimization, providing a robust foundation for application-driven development in areas such as soft robotics, deployable systems, and energy absorption.

1. Introduction

Multistable metamaterials derive their anomalous mechanical responses from engineered internal topologies rather than intrinsic material constituents [1–3]. By precisely tailoring these architectures, exotic energy landscapes characterized by negative stiffness transitions can be induced, where the system reversibly toggles between multiple discrete equilibrium states [4,5]. These transitions can be triggered through diverse external stimuli, including mechanical loading [6], impulsive shock [7,8], internal fluidic pressure [9,10], or thermal activation [11–13]. Historically dominated by bistable configurations such as von Mises trusses [14,15], these systems have become instrumental in the development of deployable structures [16], high-efficiency energy absorbers [17,18], mechanical logic gates [19–21], and adaptive robotic components [22–26].

However, the discovery of new multistable archetypes remains largely reliant on heuristic trial-and-error or the localized geometric optimization of pre-existing templates [27–29]. While these empirical approaches have successfully yielded complex behaviors such as monostable, neutrally stable [19,30], and countersnapping responses [13,31]. Furthermore, the implementation of these architectures has remained predominantly restricted to planar or quasi-planar embodiments, due to the inherent complexities of spatial design and the constraints of traditional manufacturing [32–34].

Recent breakthroughs have begun to unlock the potential of three-dimensional (3D) multistable metamaterials [35–38], demonstrating tunable multifunctional responses that include double-negative architectures, modular energy-dissipation systems, and chiral lattices with coupled rotational stability [18,29,39–41]. Yet, despite these individual advancements, the field lacks a unifying design framework capable of bridging the gap between planar and spatial domains [2,42]. The absence of a methodology that rationalizes chirality across dimensions and facilitates the systematic, controlled generation of architectures has hindered widespread industrial application and prevented the establishment of a cohesive structural taxonomy.

In prior work, we introduced a minimal *Z*-shaped topology as a

* Corresponding author.
E-mail address: p.roberjot@tudelft.nl (P. Roberjot).

https://doi.org/10.1016/j.mtcomm.2026.115963
Received 11 May 2026; Received in revised form 6 August 2026; Accepted 20 August 2026
Available online 25 August 2026

foundational base for both planar and spatial Poisson's ratio metamaterials. This led to the development of the Planar Poisson's Ratio Design Method (PPRDM) [43,44] and the Spatial Poisson's Ratio Design Method (SPRDM) [45], which utilized a discrete set of topological transformations to systematically map and discover Poisson's ratio structures.

In this work, we extend the *Z*-base concept to the domain of multistability. Although inspired by the design philosophy of the PPRDM and SPRDM, the MSMDM differs fundamentally in its objective, design seeds, and outputs. Whereas the previous methods target the systematic generation of Poisson's ratio metamaterials, the MSMDM focuses on the generation, classification, and nomenclature of multistable architectures. The introduction of bistable planar and spatial seeds, state-count prediction, multistability classification, and a dedicated naming framework constitutes a distinct design methodology rather than a direct application of the previous approaches.

We propose structural modifications to the original *Z* topology to define a planar multistable seed, Z_B, and its spatial counterpart, Z_{3B}. To establish the mechanical relevance of these seeds, we introduce an analytical pseudo-rigid-body model (PRBM) demonstrating that appropriate combinations of hinge stiffnesses and stress-free hinge rotations generate the diverse energy landscapes required for monostable, bistable and quasi-zero-stiffness. Building on this mechanically validated seed, seven topological transformations define the Multistable Metamaterial Design Method (MSMDM), a topology-driven framework for the systematic generation, classification, and nomenclature of multistable architectures. The framework complements embodiment-specific geometric optimization by identifying candidate topologies within a structured design space while remaining independent of the final realization.

Additionally, the MSMDM introduces a unified classification and naming protocol based on spatial dimensionality and a newly defined superchirality order. This allows the tracking of chirality during structural evolution and the consistent treatment of fully three-dimensional, rotating, and twisting systems. By integrating a Voronoi-based definition for unit cells, the generated topologies can be systematically tessellated into planar and spatial metamaterials. Combined with the analytical validation provided by the PRBM, the proposed framework establishes a physically grounded and topology-driven workflow for the design of multistable metamaterials. Through selected examples, including tubular, polyhedral, and countersnapping architectures, we demonstrate its ability to reconstruct established designs while generating novel families.

The remainder of this paper is organized as follows. First, we define the foundational planar and spatial bistable topologies, characterizing their fundamental kinematics as either rotational or longitudinal. The accessible mechanical behaviors of the base topology Z_B are then analytically validated using a pseudo-rigid-body model, demonstrating how variations in hinge stiffness and stress-free hinge rotations generate distinct potential energy landscapes. Second, we discuss the physical realization of multistability, outlining the accessible mechanical properties and the geometric embodiments required to achieve them. We then establish the dimensional and chirality-based classification system, which serves as the core of the MSMDM workflow and its seven topological transformations. This is followed by the introduction of a rigorous naming convention and Voronoi-based tessellation protocol, ensuring the mathematical traceability of the resulting topologies. To demonstrate the generative power of the framework, we illustrate the MSMDM through four distinct groups of architectures, showcasing its ability to both recover established designs and derive novel configurations. Finally, we characterize five specific applications of these multistable metamaterials, highlighting the emergence of complex and exotic mechanical behaviors facilitated by this systematic design approach.

2. Methods

This section introduces the Multistable Metamaterial Design Method (MSMDM), a symmetry-based framework for generating planar and spatial multistable metamaterials from minimal chiral base structures. The method defines dimensionality, chirality order, and a consistent naming protocol to classify architectures generated through topological transformations.

2.1. Z_B–Z_{3B}: Planar and spatial bistable base topologies

This work proposes a method for the design of the topology of multistable metamaterials, based on the recently developed planar (PPRDM) [43,44] and spatial (SPRDM) [45] Poisson's ratio design methods. These methods rely on the use of a chiral planar topology shaped as a *Z* (named Z_A and Z_M) and a spatial topology Z_3.

A similar approach can be taken for the development of multistable structures and metamaterials. Multistable structures can be classified by their dimension (**Section 2.4.1.**) and chirality (**Section 2.4.2.** Chirality and superchirality order). The presence of achiral and chiral multistable structures shows that a chiral base can be found and used to build a design method following the steps of the Poisson's ratio design methods. A chiral bistable base can be used as a design base for rotational multistable structures [46] and be achiralized to obtain stepper multistable structures [5]. The bistable planar chiral base named Z_B (for bistable *Z*) exists as a subset of the *Z* topology. Z_B is a three-beam structure where the beam BB' is fixed to the ground, the beam AB is has unstressed length $L_{AB} > D$ and the beam AA' is moving around a revolute joint fixed to an arm of length L allowing the structure to exhibit rotational [47] bistability (Fig. 1.**a**), if $L = \infty$, then Z_B behaves as stepper bistable structure and the beam AA', slides along a prismatic joint (Fig. 1.**b**).

The bistable base Z_B can be extended into a three-dimensional bistable base Z_{3B}, and serves as a base for twisting multistable structures [48]. Z_{3B} is composed of three beams, where BB' is fixed to the ground on a plane P_1, the beam AA' belongs to a plane P_2 parallel to P_1 and at a distance $A'B' = D$, where the line $(A'B')$ is perpendicular to the planes. The beam AA' is linked to a revolute joint at the point B' rotating around the axis $(A'B')$. The beam AB has unstressed length $L_{AB} > D$. The three beams are linked by spherical joints at points *A* and *B*, as illustrated in Fig. 1.**c**.

2.2. Realization of monostable and multistable behavior

Multistable architectures, typically synthesized from elastic beam networks, are categorized by two primary manufacturing strategies that dictate their resultant energy landscapes.

The first approach utilizes *pre-stressed beams* [49–52], where a natively straight beam of initial length $L_i > L$ is subjected to an initial deformation, via planar displacement x_0 to achieve a curved pose in which the free end is located at target length L and offset h for achiral structures actuated by a force F (Fig. 2.**a**), or a target length L and angle θ for chiral rotational topologies actuated by a moment M (Fig. 2.**b**). Pre-stressed systems are characterized by symmetric load-deflection profiles (force-displacement or moment-angle), reflecting the balanced strain energy of the initial state.

Conversely, *pre-shaped beams* [53,54] are fabricated in an intrinsically curved geometry. This configuration represents an initial state with zero strain energy, resulting in asymmetric load-deflection behavior (Fig. 2.**c**). Such asymmetry is a critical design variable; it can be leveraged to induce monostable snapping, where the multistable behavior is governed by the beam's cross-sectional geometry and curvature [27,36,55].

Within this framework, we distinguish between two classes of monostability:

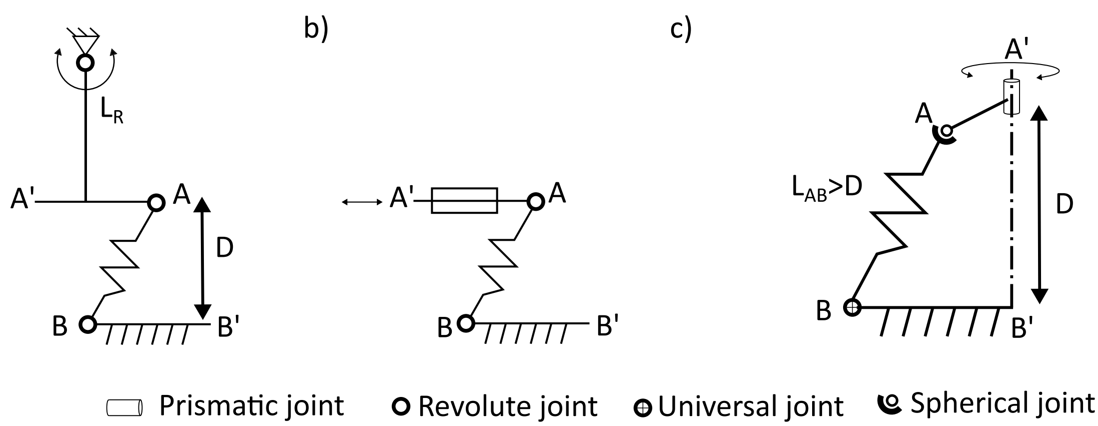

Fig. 1. Representation of the topology of the planar base Z_B as (a) a rotational bistable structure and (b) as stepper bistable structure and (c) the spatial base Z_{3B} with their remarkable points, beams and joints.

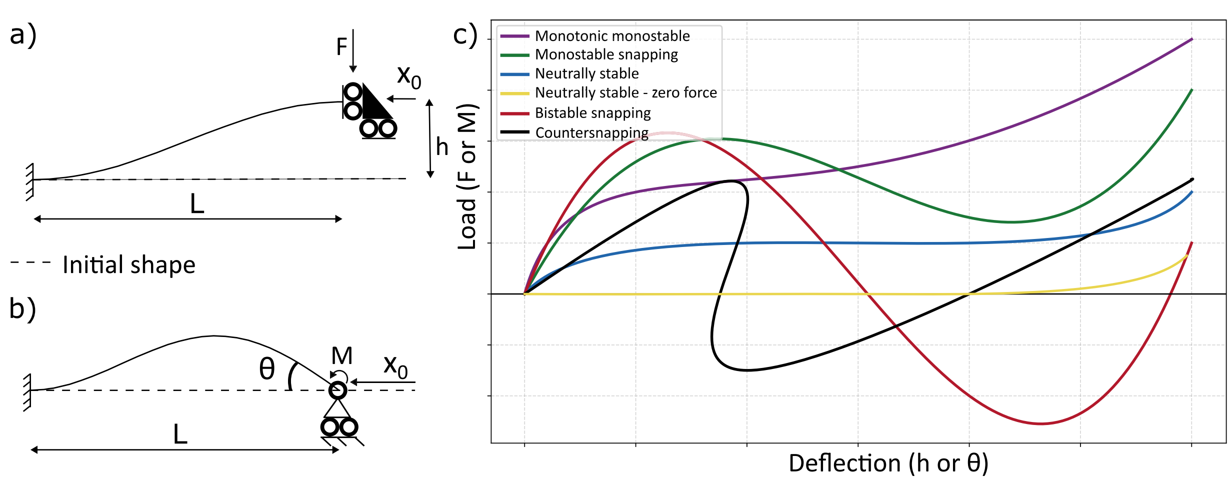

Fig. 2. Geometric configurations and mechanical responses of foundational seeds: (a) Beam shape of pre-shaped and pre-fabricated beam geometries for the achiral bistable stepper (Z_B or *Sp*); (b) corresponding geometric archetypes for the chiral rotational seed (Z_B or *Rb*). (c) Characterization of nonlinear mechanical responses, showing the evolution of force-displacement and moment-angle curves across six distinct stability regimes: the diverging monostable behaviors of pre-fabricated versus pre-shaped bistable architectures, constant force, neutrally stable, bistable snapping and countersnapping.

- *Monotonic monostable* structures: These possess a single stable equilibrium and do not exhibit snapping.
- *Non-monotonic (snapping) monostable* structures: These exhibit a non-negative, asymmetric load profile that results in a snapping transition. This behavior can be triggered via pre-shaping the beam or boundary walls [56], or through external stimuli such as thermal activation [11–13,57] and magnetic fields [5].

Architectures possessing an infinite number of equilibrium positions over a specific range of motion are defined as *neutrally stable* (Fig. 2.**c**). Neutrally stable structures are a subset of zero-stiffness structures [19, 58,59] as for the *zero-force* structures [60–62]. These are derived through the achiralization of the Z_B base into the *Ns* topology (detailed in **Section 3.2.1** .). Their load-deflection curves are monotonic and notably devoid of snapping transitions.

In contrast, *bistable structures* are defined by non-monotonic load-deflection landscapes. Symmetric bistability, where the work done during loading and unloading cycles is identical (equal areas above and below the displacement axis), is typical of pre-stressed architectures. Asymmetric bistability, arising from pre-shaped geometries, is marked by disparate energy barriers for the forward and reverse transitions. Finally, *countersnapping* or *snap-back* behaviors [13,31] emerge from the non-monotonic interaction of constituent structural elements. These are characterized by simultaneous jumps in both load and deflection, representing a higher-order instability detailed further in **Section 3.2.2** .

2.3. Analytical pseudo-rigid-body model of the Z_B topology

To analytically validate the range of mechanical behaviors accessible from the proposed Z_B topology, a pseudo-rigid-body model (PRBM) is developed [63,64]. This low-order model represents the deformation of the compliant structure using rigid links connected by torsional springs, allowing the influence of hinge stiffnesses and preloads on the potential-energy landscape to be investigated.

The centerline of the pre-curved but yet undeformed beam is approximated by the cosine profile

$$w(x) = \frac{h}{2}\left(1 - \cos\left(\frac{\pi x}{L}\right)\right) \quad (1)$$

where L is the projected beam length, h is the initial vertical distance between the beam endpoints, and $x \in [0, L]$. The beam is discretized into three rigid links connected by three torsional springs, while two rigid horizontal end segments preserve the boundary conditions, as illustrated in Fig. 3.**a**,**b**.

The kinematics of the PRBM are governed by the vector loop-closure equation

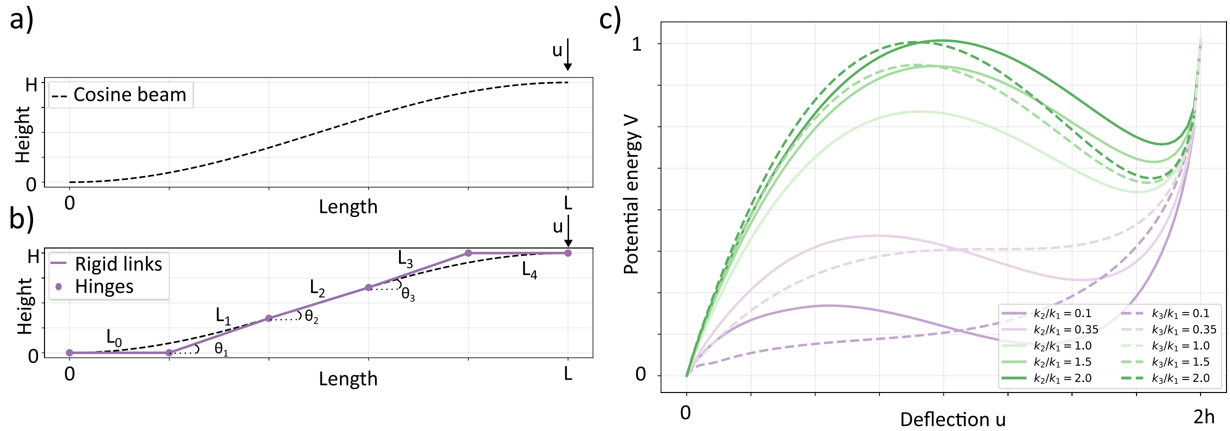

Fig. 3. Analytical pseudo-rigid-body model (PRBM) used to validate the mechanical versatility of the Z_B topology. (a) Cosine beam used to approximate the undeformed compliant beam with (b) the equivalent rigid-link model composed of three rigid links connected by three torsional springs and bounded by two rigid end segments. (c) Equilibrium path obtained by solving the loop-closure equations during a prescribed vertical displacement u, with the support distance evolving according to $H = h - u$. With representative normalized potential-energy landscapes predicted by the PRBM, illustrating monostable, bistable, quasi-zero-stiffness and nearly neutral responses obtained through variations of hinge stiffnesses and stress-free hinge rotations.

$$\sum_{i=1}^{3} L_i \begin{bmatrix} \cos(\theta_i) \\ \sin(\theta_i) \end{bmatrix} + \begin{bmatrix} L_0 + L_4 \\ 0 \end{bmatrix} = \begin{bmatrix} L \\ H \end{bmatrix} \tag{2}$$

where Hdenotes the current vertical distance between the beam endpoints. The vertical deformation is imposed through a prescribed displacement u, (Fig. 3**.a,b.**) such that

$$H = h - u \tag{3}$$

For each displacement increment, the equilibrium configuration is determined using a continuation procedure in which the central link orientation, θ_2, is treated as the continuation parameter. The remaining link orientations, θ_1 and θ_3, are obtained by solving the nonlinear loop-closure equations, and the equilibrium configuration is identified as the admissible solution minimizing the total elastic potential energy.

The total elastic potential energy of the PRBM is expressed as

$$V = \sum_{i=1}^{3} \frac{1}{2} k_i \left(\phi_i - \phi_{i,free}\right)^2 \tag{4}$$

where

$$\phi_1 = \theta_1, \phi_2 = \theta_2 - \theta_1, \phi_3 = \theta_3 - \theta_2, \tag{5}$$

where $\phi_{i,\mathrm{free}}$ denotes the stress-free hinge rotation, which may include an initial preload. The stress-free hinge rotations provide a compact representation of fabrication-induced prestress, pre-shaped geometries, or externally applied preloads, allowing different multistable embodiments to be investigated within a common analytical framework.

The PRBM demonstrates that the proposed $Z_B$topology can generate a broad range of potential-energy landscapes through variations of hinge stiffnesses and stress-free hinge rotations, as illustrated in Fig. 3**.c.** Depending on these parameters, the model reproduces monostable, asymmetric bistable, quasi-zero-stiffness, and nearly neutral responses. These results demonstrate that the proposed seed possesses the mechanical versatility required to support the subsequent development of the MSMDM.

2.4. Embodiment of bistable structures

Three motions are available through the selection of the seed and their chirality, the *rotation* motion from the seed Z_B and the chiral structure *Rb* (Rotating bistable), the *twist* motion using the spatial seed Z_{3B} and finally the *stepper* motion from the seed *Sp* that comes from the achiralisation of Z_B. The topologies, presented in **Section 2.1 .**, can be created with elastic beams, springs and joints, but also other embodiment possibilities exist and can be explored.

The seed Z_B is a chiral structure and can be used to form the chiral family *Rb* that can be found using compliant joints [65], trusses [66] and elastic beams [29,42,46]. In addition, non-contact interactions like magnets in a repulsive or attractive configuration can lead to magnet-based embodiments of the *Rb* family, that allow for larger range of motion [47]. Interestingly, because of the planar motion of a pure rotational structure origami, kirigami and shell structures have so far not been developed. Examples of embodiments of Z_B are illustrated in Fig. 4**.a.**

The spatial seed Z_{3B} showcase a twisting motion and can be embodied with elastic beams [41,48]. Dipole and magnet-based embodiments can exist as an extension of the magnet-based *Rb* structures. Origami and kirigami embodiments are possible using the Kresling pattern [67-69]. Examples of embodiments of Z_{3B} are illustrated in Fig. 4**.b.**

The seed Z_B can present a linear bistable behavior and can be achiralised in the structure *Sp* (Stepper) that presents a stepper bistable motion, one of the most common achiral bistable structure [6,35]. Magnet-based *Sp*structures have show great potential for energy trapping and absorption [28,38,70]. Kirigami embodiments are designed using geometrical frustration to enable the snap-through behavior [71-75]. In addition, shells and plates can be geometrically constrained to enable buckling and snap-through behavior [26,76-78]. Examples of embodiments of *Sp* are illustrated in Fig. 4**.c.**

The MSMDM proposes the classification of multistable topologies in four families (Z_B, Z_{3B},*Sp*, *Rb*). The topologies represent the elastic beam embodiment, however, many embodiments are possible as presented in Table 1. Five main embodiments have been shown and can be referred and named as Kirigami bistable (*Kb*), Dipole bistable (*Db*), Dipole rotational (*Dr*), origami bistable (*Ob*) and Kirigami spatial bistable (K_{3B}).

The MSMDM defines topological relationships independently of the physical embodiment used to realize the mechanism. Consequently, a given topology may be implemented through compliant beams, rigid-link mechanisms, origami, kirigami, magnetic systems, or other multistable embodiments. The choice of embodiment depends on the targeted application and desired mechanical characteristics, including stiffness, snap-through force, energy dissipation, manufacturability, and scale. The MSMDM therefore operates as a topology-generation framework that precedes embodiment selection and subsequent geometric optimization. Within the manuscript, embodiments such as *Kb*, *Db*, and *Ob* are used as representative realizations of the generated topologies. They should be interpreted as interchangeable implementation strategies

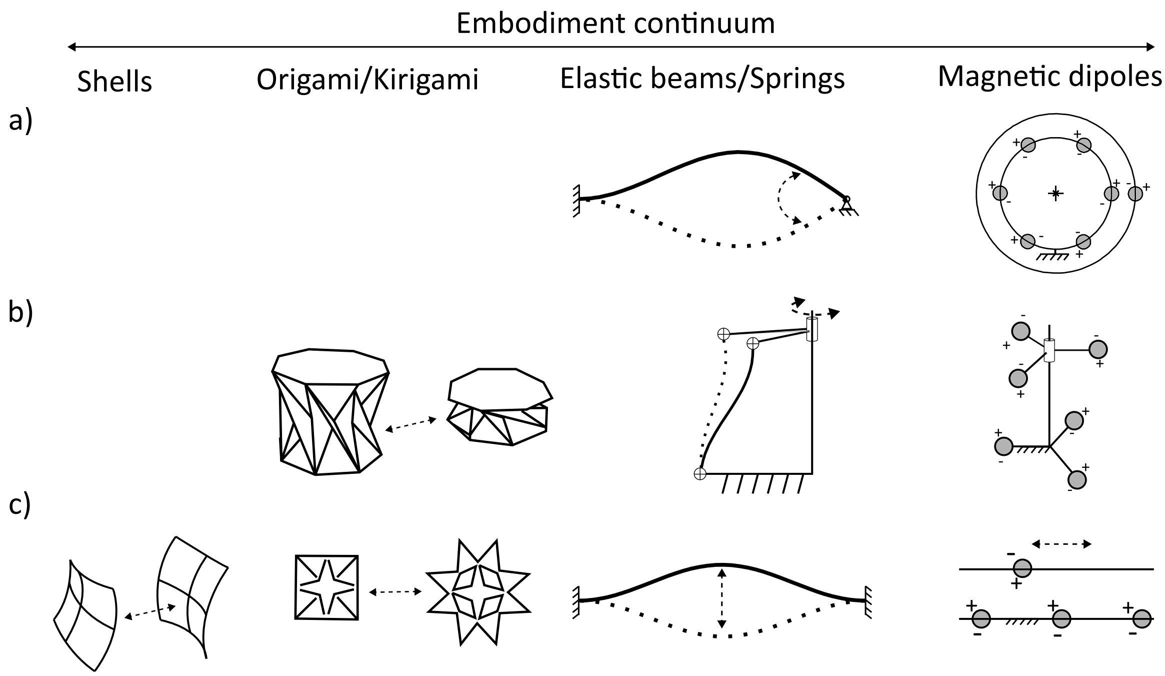

Fig. 4. Representative embodiments of fundamental multistable archetypes: (a) the rotational bistable structure (*Rb*) [29,47], (b) the torsional bistable structure (Z_{3B}) [41,68,79], and (c) the translational stepper (*Sp*). The physical realization of these topologies can be achieved through compliant mechanisms (e.g., elastic beams [24,80], origami/kirigami folding [75,81], and thin shells [82]) or via non-contact interactions, such as magnetic dipoles and attractive/repulsive force fields.

Table 1
Representative embodiments for the realization of MSMDM-generated topologies and their typical advantages and limitations. The comparison is qualitative and intended as a guideline for embodiment selection; quantitative mechanical properties, including stiffness, snap-through force, energy dissipation, and load-bearing capacity, remain dependent on the selected embodiment and geometry.

Embodiment / representative family	Principle	Typical advantages	Typical limitations
Sp / *Rb* (compliant-beam realization)	Elastic beam flexure and buckling	Simple monolithic fabrication, continuous motion, close correspondence with the ideal topological model	Material-dependent fatigue, stress concentrations, embodiment-sensitive energy barriers
Kb / K_{3B} (Kirigami bistable)	Flexure combined with strategically placed cuts in thin sheets	Lightweight, monolithic fabrication, large deformation capability	Limited out-of-plane stiffness, cut-induced stress concentrations
Ob (Origami bistable)	Folding kinematics through crease patterns	Compact deployability, large shape changes, highly programmable motion	Fold precision requirements, crease fatigue, manufacturing complexity
Db / *Dr* (Dipole bistable / rotational)	Stable equilibria generated through interacting magnetic dipoles or discrete rotational mechanisms	Tunable energy landscape, low friction, adjustable snap-through behavior	Sensitive to alignment and spacing, increased assembly complexity

rather than distinct topological families.

2.5. Multi-stable metamaterial design method (MSMDM)

The **Multi-Stable Metamaterial Design Method (MSMDM)** aims at the systematic generation and classification of multistable metamaterials. The MSMDM unifies dimensionality, chirality and symmetry-based construction within one framework.

2.5.1. Dimensional classification

The spatial distribution of their connection edges (E_N) determines the unit cells tessellation topology and honeycomb capability:

- **1.5D structures** possess collinear edges and tessellate naturally along a single axis. Both Z_B and Z_{3B} belong to this fundamental class.
- **2D and 2.5D structures** are characterized by coplanar connection edges. While fully planar (2D) structures are restricted to planar tessellation, 2.5D structures though retaining coplanar edges incorporate spatial internal geometries, enabling a transition between planar and spatial tessellation.
- **3D structures** exhibit edges distributed across three dimensions, typically inscribed within spherical or tubular geometries, facilitating fully volumetric three-dimensional tessellation.

This classification effectively decouples the geometric embedding of the structure from its internal kinematics, allowing planar and spatial architectures to be analyzed within a unified framework.

2.5.2. Chirality and superchirality order

Multistable metamaterials are also characterized by their chirality order, χ [45], defined as:

$$\chi = d - 1 - a \tag{2}$$

where d represents the minimum number of spatial dimensions required to define the structure, and a is the minimum number of independent chirality-reduction operations required to transform the considered topology into an achiral topology, as summarized in Table 2. The chirality order χ is evaluated on the resulting topology. Consequently, transformations may modify χ by introducing symmetry operations that

Table 2
Overview of the seven topological transformations constituting the MSMDM, indicating their dimensional role, effect on chirality order χ, and primary design function.

Transformation	Type	Function in MSMDM	Dimensional effect	Chirality effect
ACR (Achiralisation)	Planar / Spatial	Mirrors a chiral structure to form an achiral topology	Preserves dimension	$\chi_2 \rightarrow \chi_1$; $\chi_1 \rightarrow \chi_0$
CR (Copy-rotation)	Planar	Generates planar chiral or achiral lattices via rotational symmetry	1.5D → 2D	$\chi_1 \rightarrow \chi_1$
HCR (Hierarchization)	Planar/ Spatial	Iterates a base structure into a nested, scale-invariant topology	1.5D → 2D	χ preserved
aCR (axis copy-rotation)	Spatial	Extends achiralisation into 3D by rotation about an axis	1.5D → 2.5D / 3D	$\chi_2 \rightarrow \chi_1$; $\chi_1 \rightarrow \chi_1$
tCR (Tube copy-rotation)	Spatial	Forms tubular and prismatic spatial architectures	1.5D / 2D → 3D	$\chi_2 \rightarrow \chi_1$; $\chi_1 \rightarrow \chi_1$
LCR (Line copy-rotation)	Spatial	Generates chain-like structures	1.5D → 1.5D / 3D	χ preserved
pCR (Pyramidal copy-rotation)	Spatial	Assembles polyhedral unit cells (Platonic/Archimedean)	2D / 2.5D → 3D	$\chi_2 \rightarrow \chi_1$; $\chi_1 \rightarrow \chi_1$

reduce the number of remaining chirality-reduction operations required to reach an achiral configuration. The number χ defines the chirality type of a structure and can be classified in three categories:

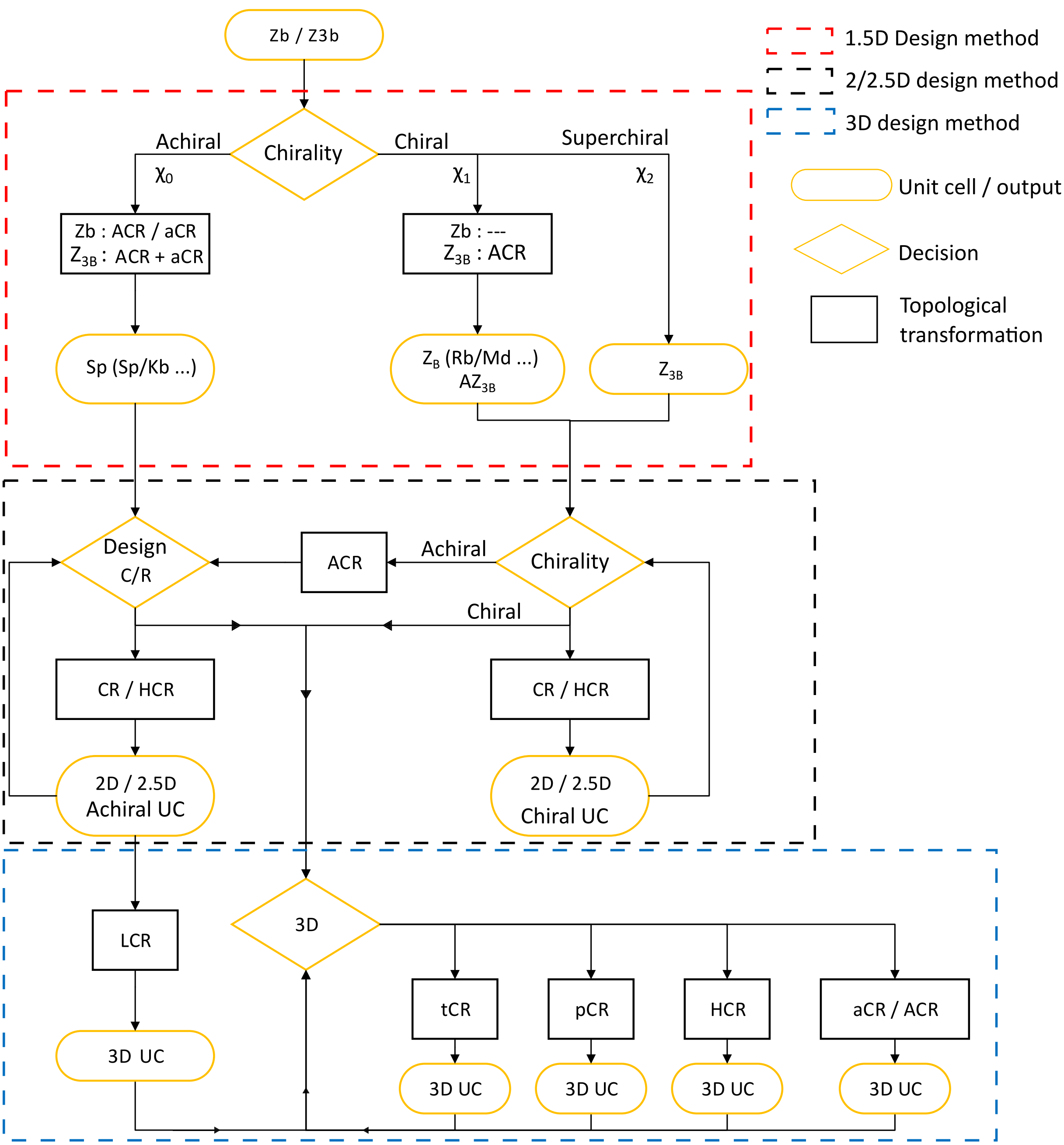

Fig. 5. Schematic overview of the Multistable Metamaterial Design Method (MSMDM). The workflow begins with the selection of either the planar bistable seed Z_B or the spatial bistable seed Z_{3B}. Chirality-reduction operations (ACR and aCR) define the chirality class (χ_0, χ_1, or χ_2), after which copy-rotation transformations (CR, HCR, aCR, tCR, LCR, and pCR) generate higher-order planar, spatial, tubular, chain-like, and polyhedral architectures. The method systematically maps candidate topologies from 1.5D seeds to 2D, 2.5D, and fully 3D multistable unit cells while preserving a traceable topological lineage.

- χ_0 denotes achiral structures (e.g., the planar structure 4.2*RSp*, illustrated in **example I** in **Section 3.1.1 .**),
- χ_1 denotes chiral structures (e.g., the planar structure Z_B, the spatial structure 6*pRb*4, see **example II** (**Section 3.1.2 .**) and **example III** (**Section 3.1.3 .**),
- χ_2 denotes spatially superchiral structures (e.g., Z_{3B}, see **example IV** in **Section 3.1.4 .**).

A superchiral structure requires multiple independent chirality-reduction operations before becoming achiral. Depending on the transformation applied, the chirality order may either be preserved or reduced, as summarized in Table 2. Within the MSMDM framework, starting from the planar Z_B seed allows for the generation of structures where $\chi \in \{0, 1\}$, whereas the spatial seed Z_{3B} enables access to the full range of $\chi \in \{0, 1, 2\}$. This hierarchy is essential for designing spatial architectures, as it distinguishes between transformations that preserve chirality order and those that actively reduce it through symmetry operations detailed in Supplementary information **SI.1**.

The MSMDM offers many possibilities for the design of multistable structures, for instance two paths lead to the same topology, this is an exceptional case detailed in **Section 3.1.4 ..** The first path uses the superchiral (χ_2) seed Z_{3B} and applies the 8-fold pCR transformation yielding the chiral (χ_1) structure 8pZ_{3B}. The second path starts from the same superchiral seed Z_{3B}. An ACR transformation first yields the chiral (χ_1) structure AZ_{3B}, after which a four-fold aCR transformation generates 4aAZ_{3B}while preserving the chirality order χ_1. Although generated through different transformation sequences, both paths lead to topologies belonging to the same chirality class (χ_1). This illustrates that the chirality order is determined by the resulting topology and not by the sequence of transformations used to generate it.

2.5.3. MSMDM workflow

The Multistable Metamaterial Design Method (MSMDM) follows a structured three-stage workflow (Fig. 5):

- **Base Selection**. The process begins with the selection of a planar chiral base structure Z_B or its spatial counterpart Z_{3B}. This choice serves as the topological seed dictating the initial degrees of freedom and the potential for multistability.
- **Chirality Management.** Topological operations such as **Achiralisation** (ACR) and **Axis Copy-Rotation** (aCR) are applied to modulate the seed's chirality.

- **Spatial Assembly.** Six **copy-rotation** transformations are employed to project the seed into higher dimensions. This comprises **Copy-Rotation** (CR) and **Hierarchization** (HCR) for planar lattices, and four spatial extensions: **Axis Copy-Rotation** (aCR), **Tube Copy-Rotation** (tCR), **Line Copy-Rotation** (LCR), and **Pyramidal Copy-Rotation** (pCR). These operations govern the final architecture (as illustrated in the design examples **Section 3**), transitioning from linear chains (1.5D) to planar lattices (2D/2.5D) or fully volumetric (3D) tessellations.

2.6. Naming, tessellation and number of states

The MSMDM allows for the creation of four main families of multistable structures with numerous possibilities for their embodiment. To bring clarity and accessibility to the design workflow we present here a compact naming convention along with a design method for the structure and tessellation of the unit cells. In addition, we propose a prediction for the number of states accessible per unit cell after transformations.

2.6.1. Topological naming convention

To ensure clarity and traceability across the vast design space generated by the MSMDM, a modular naming convention is adopted. This nomenclature functions as a concise generative syntax rather than a mere enumeration; structure names explicitly encode the topological lineage of the metamaterial. Each identifier provides information on:

- The originating base (Z_B, Z_{3B}), family (*Sp*, *Rb*) or embodiment (e.g., *Kb*, *Db*, *Dr*, *Ob* and k_{3B});
- The sequence and order of applied transformations;
- The chirality class (chiral, achiral) and design type (classical, or reciprocal);
- The resulting dimensionality of the assembly.

For example, the achiral structure 4.2*RSp* [21] comes from the Stepper (*Sp*) family that was copy-rotated in the reciprocal design (*R*) two times yielding 2*RSp* and then was copy-rotated in the higher-order four times into 4.2*RSp*, represented in Fig. 6**.b**. The chiral structure designated as 4*HRb*4 represents a planar chiral family (*Rb*) that has undergone copy-rotation (CR) four times (*Rb*4), followed by hierarchization four times into 4*HRb*4. The achiral pyramidal structure designated as 6*p*4*aSp* represents the achiral family (*Sp*) that has undergone axis copy-rotation (aCR) four times (4*aSp*), then transformed by pCR six times into 6*p*4*aSp*.

This shorthand enables an unambiguous reference to complex spatial architectures while maintaining the readability of the primary text. Representative examples and the breakdown of the encoding logic are illustrated in Fig. 6. The naming convention is applied consistently throughout the Results section, with comprehensive implementation details, prefix definitions, and extended variants reserved for Supplementary Information **SI.2**.

2.6.2. Unit cell, tessellation and honeycombs

The unit cells generated by the MSMDM follow a systematic Voronoi-based construction that maps each topological transformation into a specific tessellations. This framework ensures that the local kinematic properties of the linkage are intrinsically linked to the global tiling symmetry:

- **Planar Tessellations.** Planar transformations produce polygonal primitive cells that tile the Euclidean plane through regular or semi-regular (Archimedean) tessellations [83,84]. The Voronoi protocol ensures that the boundaries of these cells remain compatible with the expansion and contraction of the underlying multistable linkages.
- **Spatial Honeycombs.** Spatial transformations generate polyhedral unit cells—ranging from prismatic to complex Platonic and Archimedean solids—that assemble into periodic three-dimensional honeycombs [85–87].

This methodology guarantees geometric compatibility between local linkage kinematics and global tiling behavior, enabling MSMDM designs to scale seamlessly from discrete mechanisms to space-filling, multistable metamaterials. The complete geometric construction rules for unit cells, spatial cell taxonomy, and the specific Voronoi protocols are detailed in Supplementary Information **SI.3**. As an illustrative example, the LCR-derived topology 2*L*3*aSp* possesses two stable states at the isolated unit-cell level. When tessellated, neighboring cells impose additional geometric constraints through shared boundaries, allowing collective deformation modes to emerge. In this case, stable tilted configurations can appear that are not present in the isolated unit cell. Consequently, while Table 3 predicts the number of stable states associated with an individual unit cell. The tessellation may introduce additional equilibrium states arising from interactions between neighboring cells. The LCR family provides a representative example of this behavior detailed in **Section 3.1.3 .**

2.7. Prediction of the number of states at the unit cell level

The state-count predictions of Table 3 are derived from the topology

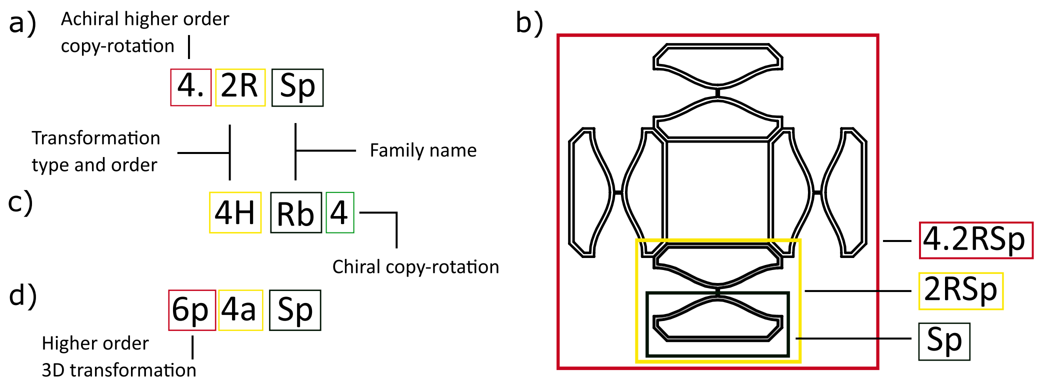

Fig. 6. Illustration of the MSMDM naming convention. The structures names encode the originating seed or family, the sequence and order of applied transformations, chirality information, and dimensionality. (a) Decomposition of the achiral structure 4.2*RSp* into its constituent descriptors. (b) Corresponding topology showing the hierarchical relationship between the base family *Sp*, the intermediate structure 2*RSp*, and the final structure 4.2*RSp*. (c) Example of a hierarchical chiral structure (4*HRb*4) generated through the hierarchization transformation (HCR). (d) Example of a spatial structure (6*p*4*aSp*) generated through axis copy-rotation (aCR) followed by pyramidal copy-rotation (pCR). The notation provides a compact representation of the full topological generation pathway, allowing the topology of a structure to be reconstructed directly from its name.

Table 3
Prediction of the topological number of accessible stable configurations at the unit-cell level for the transformations applied to the seeds and families with *n* the multiplicity within a single transformation and *N* the higher-order repetition level.

Seed	Planar transformations			Spatial transformations			
	ACR	**aCR**	**HCR**	**aCR**	**pCR**	**tCR**	**LCR**
Z_B	S $(Z_B \rightarrow Sp)$	$S(Z_B \rightarrow \mathrm{Rb})$	N/A	S $(Z_B \rightarrow Sp)$	N/A	N/A	N/A
Rb	$2 \times S$	S^n	S^2	S^n	S^n	S^n	$2 \times S$
Sp	S	$[n, S^n]$	$S^{(N+1)}$	S^N	S^n	S^n	S
Z_{3B}	S	N/A	N/A	S	M vertices	N/A	N/A

of the transformations rather than from an energy-based analysis. Transformations such as ACR and CR preserve the number of stable states because they modify symmetry without introducing additional independent bistable elements. In contrast, transformations such as aCR, pCR and HCR replicate bistable substructures that may switch independently, leading to a multiplicative increase in the number of accessible states. Consequently, Table 3 should be interpreted as a prediction of the topological number of accessible stable configurations at the unit-cell level. The actual realization, stability, and energetic accessibility of these states remain dependent on the selected embodiment and subsequent geometric optimization.

The bistable seeds Z_B and Z_{3B} possess, by definition, two stable states. The topological transformations may either modify the chirality of the response (e.g., rotational to translational) or increase the number of accessible stable configurations through an increase in topological complexity. Table 3 presents an overview of the number of states predicted for each transformation applied to a seed with S stable states, where S is the number of states of the base, with n the multiplicity within a single transformation and N the higher-order repetition level. A transformation applied to a seed transforms the seed into an element of a family and is denoted: S $(Z_B \rightarrow Sp)$. Further transformations should be continued at the family line *Sp*, in that case. Regarding the pCR transformation of Z_{3B}, the M vertices represent the number of faces of the polyhedron generated by the transformation.

For example, the aCR transformation applied four times to the seed Z_B preserves the number of states $S = 2$ and generates the structure *Rb*4. Applying aCR four additional times to *Rb*4 yields the higher-order structure *Rb*4.4, which contains four independents *Rb*4 substructures. Since each substructure possesses two stable states, the resulting topology exhibits $S^n = 2^4 = 16$ accessible topological configurations.

Although the unit-cell state count can be predicted topologically, tessellation may introduce additional equilibrium states through interactions between neighboring cells and may also generate novel forms of multistability, such as stepper-to-bending [88] or stepper-to-twist [21].

2.8. Scope of the method

Using this structured workflow, the MSMDM generates three planar and one spatial family of regular multistable metamaterials. These foundational families can be further extended into a diverse array of embodiments and architectures.

The MSMDM framework serves three purposes: (i) a generative design framework for the systematic creation of multistable topologies, (ii) a classification framework based on dimensionality and chirality order, and (iii) a naming protocol for the consistent identification of generated structures. The framework is not intended to predict force-displacement responses, energy barriers, or load-bearing capabilities, which remain dependent on the selected embodiment and subsequent geometric optimization. Instead, the method prioritizes topological generation over specific geometric optimization, establishing a rigorous design space for metamaterials characterized by translational, rotational, and torsional multistability.

By focusing on the underlying symmetry and connectivity, the MSMDM provides a scalable framework for discovering novel mechanical behaviors across different scales. Detailed descriptions of the seven topological transformations, along with their representative applications and mechanical implications, are presented in **Section 3** .

3. Results

This section demonstrates the generative capacity of the Multistable Metamaterial Design Method (MSMDM) in synthesizing planar and spatial multistable metamaterials from minimal topological seeds. Rather than providing an exhaustive catalog of the design space, this analysis focuses on three primary objectives: (i) the functional role of the seven topological transformations in defining structural behavior; (ii) representative design pathways that recover established architectures and reveal novel configurations; and (iii) selected classes of metamaterials tailored for specific mechanical applications.

3.1. Design examples

3.1.1. Example I - Multistable planar achiral structures

Starting from the planar base Z_B the application of the achiralisation transformation (ACR) leads to the achiral topology *Stepper bistable* (*Sp*). The *Sp* topology can be embodied in various manners such as kirigami and using repulsive or attractive magnets. Using the *Sp* topology in the MSMDM workflow, it is possible to design planar multistable structures by application of the copy-rotation (CR) transformation in the classical and reciprocal designs (Fig. 7**.a-d**). The structure *Sp* can be copy-rotated in the classical design four times for instance yielding the structure 4*CSp* [89], or in the reciprocal way two times to form the structure 2*RSp* [36, 90-92] and four times as the structure 4*RSp*. The frames of 4*RSp* can be linked together in a variation that allows for the center body to have *N* stable positions (Fig. 7**.e**), in order to achieve such a structure, the opposed *Sp* bases have to be in inverted states, for even *N* and at least one of the *Sp* base have to be in a different state for odd *N* [93]. In addition, a copy-rotated structure can be copy-rotated to the higher-order (HO), meaning that the copy-rotation can be applied with many iterations leading to more complex structures such as 4.2*RSp* [21], as illustrated in Fig. 7**.f**.

3.1.2. Example II - Novel chiral structures

Using the planar seed Z_B as a chiral base to form the family *Rb* (illustrated in Fig. 8**.a**), the copy-rotation transformation can be apply at the center of rotation O_R forming, for instance, the bistable chiral structure *Rb*4 illustrated in Fig. 8**.b**. The hierarchization transformation can be applied to the structure *Rb*4 for instance four times yielding the topology 4*HRb*4 [29], illustrated in Fig. 8**.c**. The self-hierarchized topology leads to a fractal design or self-replicating structure where the stiffness of each layer could be controlled by the shape, dimension and geometry of the flexures. In the general case of hierarchical structures the stiffness of each layer can also be controlled by the number of repetition of the copy-rotation, for instance, the structure 4*HRb*3 possesses four flexures on the outer layer and three in the inner one, on the contrary 3*HRb*4 possesses three flexures on the outer layer and four in the inner one. For flexures of identical geometry and dimensions, where only the number of flexures changes the stiffness of the layer, the deformation's sequence varies between the two structures for an overall identical number of steps and behavior.

The *Rb* family can be used as a base for spatial transformations such as the *pyramidal copy-rotation* (pCR) *tube copy-rotation* (tCR) and *axis copy-rotation* (aCR). For instance, the structure 4*HRb*4 can be transformed by pCR six-fold leading to the design of a cubic structure 6*p*4*HRb*4 where each face is a hierarchical chiral structure, as illustrated in Fig. 8**.d**. 6*p*4*HRb*4 can be used as a cubic unit cell, however, because of the rotational multistable faces the honeycomb created can only be used on the outer faces of the honeycomb. Such structures could show potential in chain tessellations for computational or positioning purposes for instance in twisting the main chain and orienting the sided end-effectors, some examples of such applications are shown in **Section 3.2.4 .** Multistable robots and energy trapping

3.1.3. Example III - Spatial structures based on Z_B

The axis copy-rotation (aCR) is a topological transformation that enables the transformation from the planar chiral seed Z_B (Fig. 9**.a**) to a 2.5D structure that can be tessellated in the plane of the base and in a line from the edge $E = B$ of the structure. The aCR transformation is illustrated in Fig. 9**.b** with the structure 3*aSp* composed of three flexures allowing the structure to be deformed into an up and down position. Such structures can be tessellated in the plane in two ways, the first is to use the created structure as a unit cell, for instance the structure 4*aSp* is a square structure that is tiled in a regular tiling (Fig. 9**.d**). Second, the 2.5D structure can be copy-rotated to the higher order, similarly to a planar structure, for instance 4.4*aSp* illustrates the process in Fig. 9**.e**. The two tessellations allow for modifications of the deformation pattern

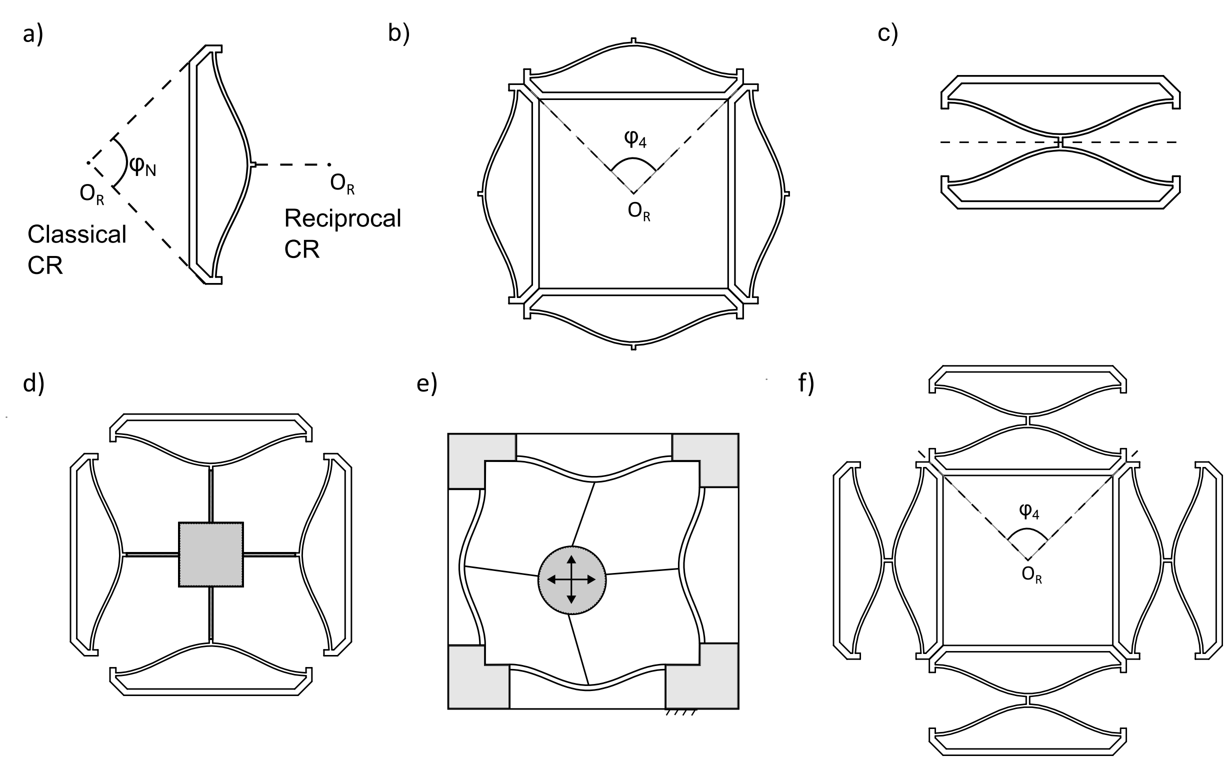

Fig. 7. Illustration of the topology of (a) the achiral structure *Sp* represented with the location of the points O_R in the Classical and Reciprocal design scenario. The planar *Sp* structure can be transformed by copy-rotation (CR) in (b) the classical design four times in the structure 4*CSp* and in the reciprocal design (c) two times yielding the structure 2*RSp* and (d) four times in the structure 4*RSp*. The copy-rotated structure 4*RSp* (e) can have the four frames connected leading the central body to possess four internal stable configurations. A structure can undergo higher-order copy-rotation, for instance (f) 2*RSp* can be copy-rotated four times yielding 4.2*RSp*.

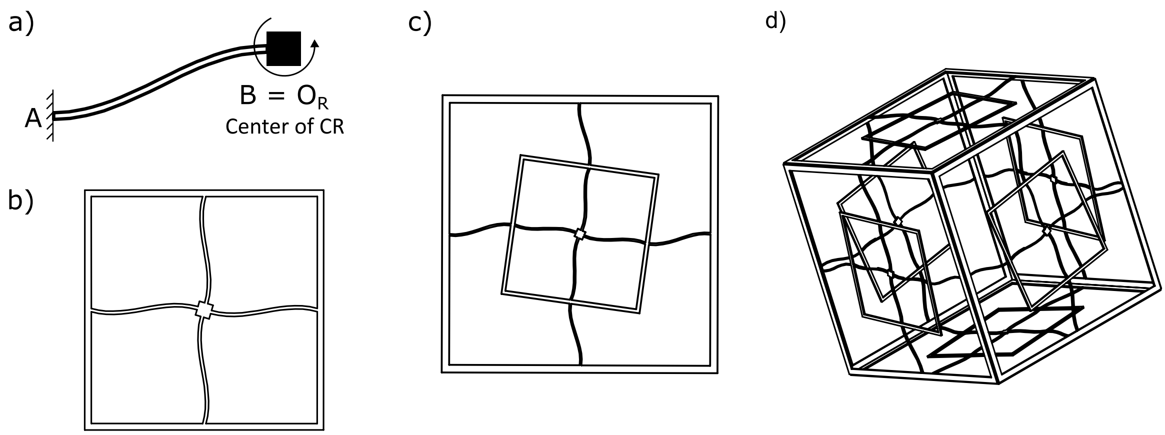

Fig. 8. Topological transformations of chiral structures: (a) geometric definition of the chiral seed Z_B (rotational archetype, *Rb*) indicating the center of copy-rotation O_R. (b) The assembly *Rb*4, resulting from a four-fold copy-rotation of the base *Rb*. (c) Evolution through hierarchization, where a four-fold HCR transformation yields the two-layered fractal 4*HRb*4 architecture, characterized by four distinct stable states. (d) Volumetric projection via pyramidal copy-rotation (pCR), illustrated by the cubic assembly 6*p*4*HRb*4 which utilizes the hierarchical structure as a functional base for 3D tessellation.

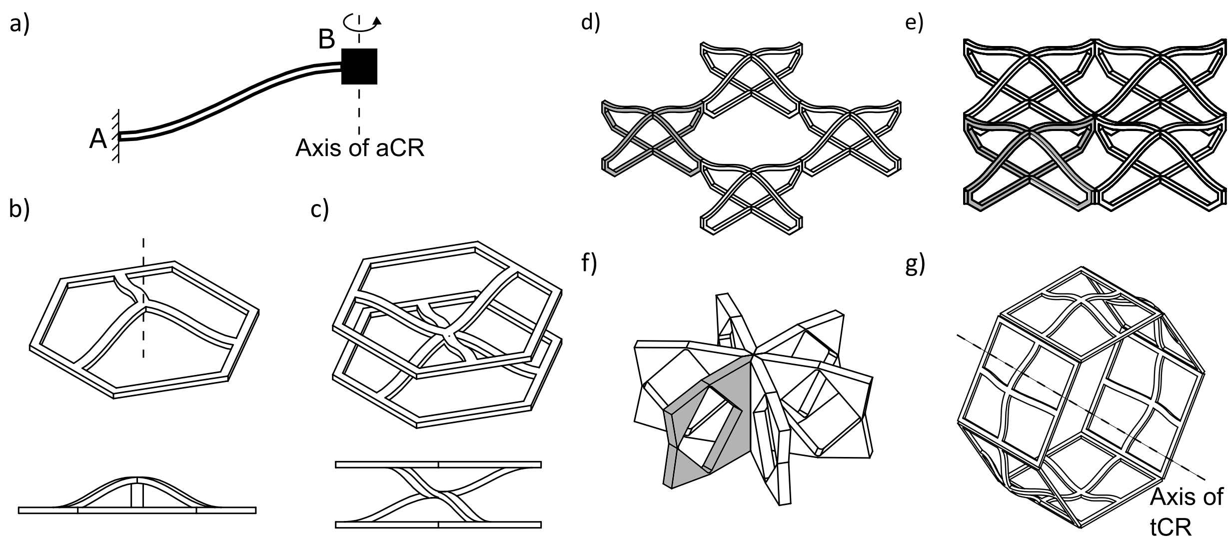

Fig. 9. Volumetric and linear transformation of axial copy-rotated structures: (a) geometric definition of the Z_B base with the indicated axis of copy-rotation (aCR). (b) The three-fold axial assembly 3*aSp*, which can be further extended via line copy-rotation (LCR) to form (c) the structure 2*L*3*aSp*. The LCR-derived topology provides a representative example where tessellation may introduce additional collective deformation modes. While the isolated unit cell remains bistable, interactions between neighboring cells can generate additional tilted equilibrium configurations that are not present in the isolated unit cell. (d) Planar tessellation of axial units, illustrated by the 4*aSp* configuration, and (e) the application of higher-order copy-rotation resulting in the complex 4.4*aSp* topology. (f) Embodiment-specific transformation of the kirigami base (Kb) into the six-fold axial classical structure 6*aCKb*. (g) Extension into tubular geometries via tube copy-rotation (tCR), exemplified by the 6*t*4*aSp* architecture. The figure illustrates how aCR, LCR, and tCR generate planar, chain-like, tessellated, and tubular multistable families from a common axial design principle.

and could lead to specific applications.

The tessellation of certain unit cells has been showing the gain of additional stable positions not present in the unit cell such as tilted stable positions. This is the case of the tessellation of structures formed from the Line copy-rotation (LCR). The LCR transformation (codded 2*L*) combines two transformations, first, it mirrors a structure and second, the mirrored structure is rotated by an angle $\varphi_N = \frac{360^\circ}{2N}$ with *N* the order of the base, for instance, the structure 2*L*3*aSp* [88] illustrated in Fig. 9.**c** possesses a bistable behavior such as 3*aSp* however, it also possesses a continuous monostable tilting behavior. In addition, when tessellated 2*L*3*aSp* exhibit also tilting stable behaviors in three directions.

The aCR transformation could be applied to various embodiments such as the kirigami *Kb* structure Fig. 9.**f** allowing for potential applications and various designs for instance with the structure 6*aKb*.

After the application of the aCR transformation, the structures can be employed in other spatial transformations for instance with the tCR [36] the topology 4*aSp* can form a tube with six faces as 6*t*4*aSp*. Two types of tubes can be built, the multistable longitudinal tubes that use the multistable behavior to expand or contract in the direction of the tube, and the multistable radial tubes that use the multistable behavior to expand or contract in the radial direction. The combination of the longitudinal and radial tubes can be done in two ways, first is to alternate the use of a longitudinal and radial ring for instance alternating 6*t*4*aSp* and 6*t*2*RSp*, illustrated in Fig. 9.**g**. Second, is to use a unit cell before tCR that is multistable in the two directions, for instance 4*CSp*, 4*RSp* and 6*p*4*aSp* show great potential as they decouple the multistable directions.

It is also possible to gain in degrees of freedom with the addition of irregularities and angles in the design in order to have, for instance a bistable *Sp* structure where the end effector is not moving in a vertical or horizontal straight line but follows a curve [94]. Such irregular design can be used in a spatial configuration after tCR transformation for instance as in the structure 4*tSp* presented in [79], where the angled orientation of the end-effector allows for a twisting (both rotation around the z-axis and change in height) bistable motion.

3.1.4. Example IV - Spatial structures based on Z_{3B}

The seed Z_{3B} (Fig. 10.**a**) can be used as a starting point in the MSMDM design workflow. The superchiral χ_2 structure show a spatial rotational bistable behavior, it can be transformed with spatial transformations, for instance the axis copy-rotation (aCR) that is reducing the chirality order to χ_1 can yield, for a three-fold transformation the structure $3aZ_{3B}$ [48] with the angle $\varphi_3 = 120^\circ$ between each Z_{3B} element. The structure is presented in Fig. 10.**b** where the distance D is fixed and to be bistable with the use of elastic beams the condition where the distance D has to be smaller than the length L of the beams. We note that the achiralisation (ACR) about one of the planes containing the fixed based and the tessellation along the axis of D is the same transformation. Indeed, because the bistable structure possesses two states one of them is a chiral continuation of the chain while the second is the equivalent of the achiralisation transformation.

The spatial seed can be used in the pCR transformation, for instance the structure $8pZ_{3B}$ [95] is illustrated in Fig. 10.**c** and shows eight spatial copy-rotation of the base Z_{3B}. This structure possesses eight stable configurations and could potentially be hierarchized to create a fractal-like structure such as $8H8pZ_{3B}$. The MSMDM allows for the construction of many topologies and following the many paths some structures can be created from at least different paths leading to two names for the same structures. For instance, the spatial base Z_{3B} can be achiralised (ACR) into AZ_{3B} and then transformed four-fold by axis copy-rotation (aCR) into $4aAZ_{3B}$ which is the exact same structure as $8pZ_{3B}$. Following the aCR path leads to designing *prism-like* spatial multistable structures, whereas the pCR path leads to *platonic solid-like* structures. Furthermore, when multiple transformation paths yield an identical topology, which remains a rare exception, a canonical name should be selected based on the shortest transformation sequence from the seed structure. Under this convention, $8pZ_{3B}$becomes the preferred designation, while $4aAZ_{3B}$ is treated as an equivalent alternative representation.

3.2. Applications for multistable metamaterials

Beyond isolated configurations, the MSMDM facilitates the systematic discovery of several prominent metamaterial families, each possessing unique mechanical signatures. To demonstrate the versatility of this framework, five representative applications are characterized herein, highlighting the practical utility of these multistable architectures.

3.2.1. Neutrally stable structures

Multistable architectures are characterized by a negative stiffness transition during the snap-through between equilibrium states. Conversely, structures engineered with a force-displacement (or moment-angle) plateau exhibit a zero-stiffness regime; within this range, the structure maintains a constant restorative force (or moment) across a continuous interval of deformation [19,30,62,96,97].

Within the MSMDM framework, two distinct topological pathways enable the design of such multi-stable behavior:

- **Chiral Architectures:** For chiral systems, the $Rb4$ configuration has been demonstrated to produce zero-stiffness plateaus when realized with optimized beam profiles [30]. By iterating the design through the HCR transformation (e.g., $4HRb4$), multiple zero-stiffness regions can be embedded into the rotational moment-angle response, creating a discretized multi-step energy landscape.
- **Achiral Architectures:** For achiral multi-stability, an achiralisation (ACR) process is applied to the Z_B seed, giving rise to the neutrally stable (Ns) family. As illustrated in Fig. 11.**a**, the axis of achiralisation A_R passes through point B and remains normal to the BB' base. To activate the zero-stiffness state, the Ns structure requires specific preloading (Fig. 11.**b,c**); integrating a bistable unit at the boundary allows for a tunable interface that can switch the global response between multi-stable and monostable regimes [19,58].

Finally, while the Z_{3B} spatial seed theoretically provides a topological foundation for multi-stable volumetric bases, no existing literature has yet characterized this specific embodiment, marking a potential frontier for the MSMDM application.

3.2.2. Countersnapping structures

Within the MSMDM framework, such a system is encoded as a hybrid assembly of Sp units configured in both bistable and monostable regimes connected in series, paired with a strain-stiffening meiotic structure $2CLb$ [44,45] arranged in parallel. To facilitate higher-order design, this coupled system can be abstracted as a functional macro-seed denoted L_{CS} (Longitudinal Counter-Snapping). This abstraction enables its seamless integration into the MSMDM workflow and allows the generation of higher-order architectures such as the tubular countersnapping lattice $4tL_{CS}$. The countersnapping behavior associated with this

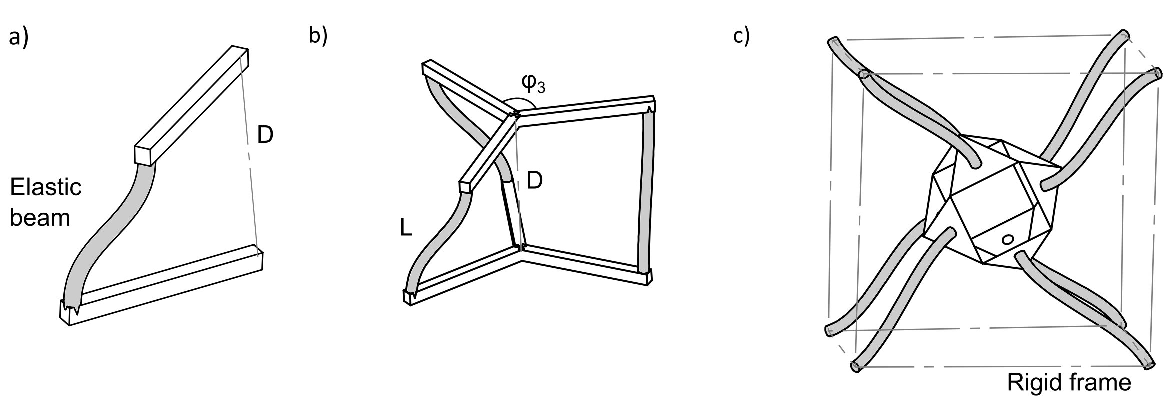

Fig. 10. Volumetric evolution of spatial multistable architectures generated from the superchiral seed Z_{3B}. (a) Geometric definition of the spatial seed Z_{3B}, realized through a compliant elastic beam constrained by a fixed inter-frame distance D. (b) Three-fold axial assembly $3aZ_{3B}$ generated through axis copy-rotation (aCR). (c) Volumetric projection via pyramidal copy-rotation (pCR), resulting in the octahedral architecture $8pZ_{3B}$. The figure also illustrates an exceptional case in which two distinct transformation sequences converge to the same final topology. The structure $8pZ_{3B}$ may be generated directly from Z_{3B} through an eight-fold pCR transformation, or equivalent through achiralisation (ACR) of the seed to obtain AZ_{3B}, followed by a four-fold aCR transformation yielding $4aAZ_{3B}$. Although generated through different transformation pathways, both structures belong to the same chirality class (χ_1), illustrating that chirality order is determined by the resulting topology rather than by the transformation history. The figure highlights the ability of the MSMDM to generate equivalent spatial architectures through alternative topological pathways while maintaining a consistent chirality classification.

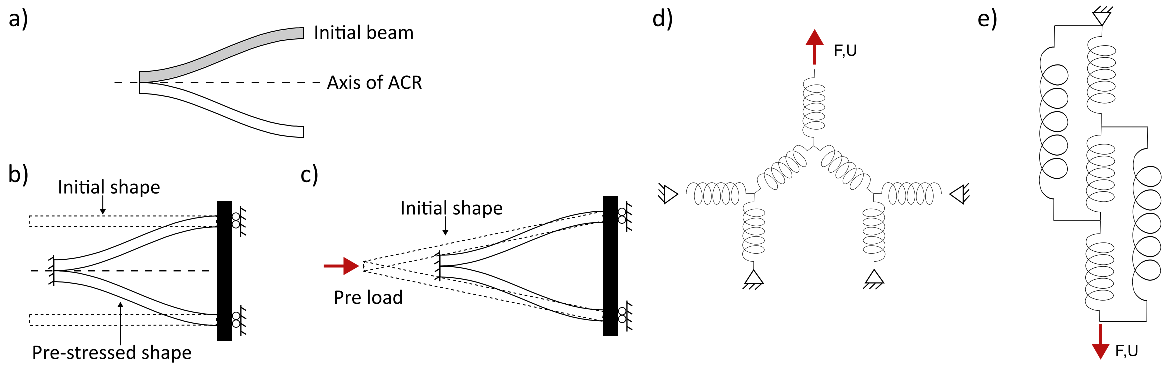

Fig. 11. (a) Topological derivation of the neutrally stable *Ns* architecture through the achiralisation (ACR) of the Z_B seed. (b) Physical embodiment of a neutrally stable response utilizing pre-stressed, disconnected beam assemblies. (c) Realization of neutral stability via monolithic pre-shaped beams, demonstrating the geometric tuning of the energy landscape. (d, e) Equivalent spring-mass kinematic models representing two distinct network architectures designed to facilitate snap-back instabilities and discretized transitions [13,31].

topology, including contraction under extension, has been demonstrated in the literature [13,31]. This exotic mechanical response is orchestrated by a network of interconnected nonlinear, monotonic, and strain-stiffening units, as characterized in Fig. 11**.d,e**. Within the MSMDM, the L_{CS} macro-seed serves as a compact topological representation that enables the systematic generation and classification of countersnapping architectures.

3.2.3. Out of plane buckling and shape morphing

Multistable unit cells possess the ability to expand or contract in one direction while keeping the same dimension in the other directions usually because of the presence of a rigid frame. When a planar multistable metamaterial is enclosed in a rigid frame, the only possible deformation of the unit cells is out of plane. It is therefore possible to program the deformation of a multistable surface into a volume as a whole or by region. This functionalities may lead to potential applications in the development of deployable mechanisms [9,98] and shape morphing surfaces and structures [94,99].

3.2.4. Multistable robots and energy trapping

Multistable structures are characterized by the existence of at least two distinct stable configurations, requiring energy input only to navigate the transition between stable states. This intrinsic multistability has sparked significant interest in the development of multistable robotic systems [25,26,100] and articulated arms [30,40]. By increasing the number of constituent unit cells, these systems can approximate continuous motion and maintain intermediate poses indefinitely without continuous power consumption or active control.

Furthermore, the integration of multistable mechanisms into continuum robots and architected metamaterials introduces structural locking capabilities and serves as a platform for energy-trapping mechanisms. These properties demonstrate high potential for applications in impact mitigation and programmable shock absorption [8,101].

3.2.5. Computational application

Multistable structures offer a compelling physical alternative to electronic transistors, enabling the development of mechanical computing systems where information is stored and processed through structural states rather than electrical charges [5,100,102–105]. By assigning binary values to distinct stable configurations, these architectures can function as non-volatile memory cells that retain data without a continuous power supply.

When integrated into complex networks, the snap-through transitions between these states can be used to execute combinatorial logic operations (AND, OR, NOT) and sequential processing [106,107]. Beyond binary logic, the nonlinear energy landscapes of multistable metamaterials are increasingly being leveraged for physical reservoir computing, where the structural response to mechanical inputs is used to perform complex pattern recognition and signal processing tasks directly within the material's hardware.

4. Discussion

This work introduces the Multi-Stable Metamaterial Design Method (MSMDM) as a unified, topology-based framework for the systematic generation, classification, and nomenclature of planar and spatial multistable metamaterials. Built upon the minimal bases Z_B and Z_{3B} and a limited set of seven topological transformations, the MSMDM provides a constructive pathway to design multistable, neutrally stable and countersnapping structures across chirality and dimension.

A primary contribution of the MSMDM is its generative capacity; rather than iterating upon a localized geometry or targeting a narrow mechanical objective, the framework systematizes a vast design space through the lens of symmetry, topological connectivity, and fundamental kinematic principles. Consequently, the results presented herein focus on a strategic subset of illustrative transformations and archetypes. These examples demonstrate the framework's ability to recover established architectures found in the literature while simultaneously unveiling previously undocumented spatial families.

The classification system centered on dimensionality and chirality resolves long-standing ambiguities between planar, quasi-planar, and truly spatial Poisson's ratio metamaterials. Specifically, the introduction of the *superchirality order* χ provides a mathematically compact metric to distinguish between planar-chiral, spatial-chiral, and fully achiral architectures. This parameter enables systematic tracking of chiral evolution throughout successive topological transformations. Such a distinction is vital when projecting planar design principles into three-dimensional space, where the transition to achirality often necessitates multiple independent, non-commutative symmetry operations.

While the MSMDM prioritizes the development of high-symmetry reference architectures, it simultaneously establishes a robust secondary design layer through the introduction of structural irregularities. By modulating base geometric parameters, employing non-integer transformation orders, or implementing heterogeneous tessellations, the framework facilitates the engineering of graded mechanical responses, directional anisotropy, and localized functional zones in a metamaterial structure.

Furthermore, the physical embodiment of these topologies serves as a critical design variable, enabling the calibration of specific phenomena such as delayed snap-through, monostable transitions, and stimulus-responsive behavior. While established analytical beam models currently guide the design of specific topologies with predictable kinematics, the broader design space remains fertile for exploring novel geometries and embodiments (that may lead to novel families) that may unlock unconventional snapping dynamics and energy dissipation profiles.

The versatility of the MSMDM has been substantiated through the characterization of complex emergent behaviors, specifically the realization of *countersnapping* in translational stepper architectures and the achievement of discretized energy landscapes in neutrally stable rotational topologies. While the framework systematically generates a vast array of spatial and high-order chiral configurations, the MSMDM reveals a particularly promising design space for the development of multi-axial rotational mechanisms and *twist-countersnapping* architectures. Such structures, which couple axial rotation with longitudinal contraction, represent a significant frontier for future experimental validation and provide a roadmap for the development of multi-functional, twisting neutrally stable systems.

The MSMDM serves as a generative methodology that facilitates both the design of established architectures and the systematic creation of novel multistable metamaterials from fundamental planar and spatial seeds. While this framework does not claim to define the absolute limit of all possible multistable topologies, it is noteworthy that a broad class of reported multistable architectures can be successfully mapped and classified within the current MSMDM parameters. This suggests a high degree of topological completeness and reinforces the framework's utility as a comprehensive design tool. In addition, this manuscript, with the establishment of the MSMDM as its primary goal, presents a significant number of references that could serve as a base for a review.

Overall, the MSMDM establishes a unifying nomenclature and a streamlined workflow for the development of planar and spatial multistable metamaterials. By decoupling topological generation from localized mechanical optimization, the method provides a standardized foundation upon which computational simulations, experimental validations, and application-specific refinements can be systematically executed. Future research will prioritize the quantitative mechanical characterization of these topologies, the development of additive-manufacturing-ready embodiments, and the integration of MSMDM-derived architectures into functional systems ranging from high-efficiency energy absorbers and deployable structures to adaptive soft robotic components.

5. Conclusion

This work establishes the Multistable Metamaterial Design Method (MSMDM) as a unified, topology-based framework for the systematic generation, classification, and nomenclature of planar and spatial multistable metamaterials. By fundamentally re-engineering the chiral minimal structures used in auxetic design, we introduce the planar chiral bistable seed Z_B and its volumetric extension Z_{3B}. We demonstrate that a discrete library of seven topological transformations is sufficient to both reconstruct a broad class of reported multistable architectures and generate novel multistable structures. The MSMDM shifts the design paradigm from localized geometric optimization to global topological generation, defining a vast design space governed by dimensionality and chirality. A formalized naming protocol ensures mathematical traceability across all derived topologies, while the introduction of the "superchirality" parameter provides a robust metric for treating planar and spatial chirality within a consistent analytical framework. Through representative examples of multistable structures including multistable, constant force, neutrally stable and countersnapping structures, we show that the MSMDM captures existing multistable structures while enabling the design of novel planar and spatial topologies. By defining unit cells through a Voronoi-based formalism, these structures are inherently compatible with planar and spatial tessellation. Ultimately, the MSMDM offers a generative and extensible methodology that bridges the gap between abstract topology and functional mechanical metamaterials, providing a foundation for future numerical optimization and application-driven structural exploration.

CRediT authorship contribution statement

Jonathan B. Hopkins: Validation, Supervision, Methodology. **Just L. Herder:** Validation, Supervision, Methodology. **Pierre Roberjot:** Writing – review & editing, Writing – original draft, Visualization, Methodology, Investigation, Formal analysis, Conceptualization.

Declaration of Competing Interest

The authors declare that they have no known competing financial interests or personal relationships that could have appeared to influence the work reported in this paper.

Acknowledgment

This publication is part of the project Mechanical Metamaterials for Compact Motion Systems (MECOMOS), project number 18940 of the Open Technology Program financed by the Dutch Research Council (NWO).

Appendix A. Supporting information

Supplementary data associated with this article can be found in the online version at doi:10.1016/j.mtcomm.2026.115963.

Data availability

No data was used for the research described in the article.

References

[1] S.E. Rodríguez, E.P. Calius, A. Khatibi, A. Orifici, R. Das, Mechanical metamaterial systems as transformation mechanisms, Extrem. Mech. Lett. 61 (2023) 101985, https://doi.org/10.1016/j.eml.2023.101985.
[2] R. Xu, et al., The design, manufacture and application of multistable mechanical metamaterials-a state-of-the-art review, Int. J. Extrem. Manuf. 5 (4) (2023) 042013, https://doi.org/10.1088/2631-7990/acf96a.
[3] X. Guo, Y. Xu, N. Zhu, H. Xu, Multistable mechanical metamaterials with compatible sensitive actuation and high stability, Extrem. Mech. Lett. 83 (2026) 102450, https://doi.org/10.1016/j.eml.2026.102450.
[4] M.A. Pucheta, A. Cardona, Design of bistable compliant mechanisms using precision–position and rigid-body replacement methods, Mech. Mach. Theory 45 (2) (2010) 304–326, https://doi.org/10.1016/j.mechmachtheory.2009.09.009.
[5] T. Chen, M. Pauly, P.M. Reis, A reprogrammable mechanical metamaterial with stable memory, Nature 589 (7842) (2021) 386–390, https://doi.org/10.1038/s41586-020-03123-5.
[6] A. Rafsanjani, A. Akbarzadeh, D. Pasini, Snapping mechanical metamaterials under tension, Adv. Mater. 27 (39) (2015) 5931–5935, https://doi.org/10.1002/adma.201502809.
[7] T. Frenzel, C. Findeisen, M. Kadic, P. Gumbsch, M. Wegener, Tailored buckling microlattices as reusable light-weight shock absorbers, Adv. Mater. 28 (28) (2016) 5865–5870, https://doi.org/10.1002/adma.201600610.
[8] H. Ma, et al., Energy dissipation and shock isolation using novel metamaterials, Int. J. Mech. Sci. 228 (2022) 107464, https://doi.org/10.1016/j.ijmecsci.2022.107464.
[9] Y. Veksler, E. Ben-Abu, A.D. Gat, Fluid-driven director-field design enables versatile deployment of multistable structures, Adv. Intell. Syst. 6 (8) (2024) 2400179, https://doi.org/10.1002/aisy.202400179.
[10] A. Rezanejad, M. Mousa, Y. Wang, M. Adlerstein, J. Yao, A.E. Forte, Vacuum–laser fabrication of programmable soft actuators (vol. n/a, no. n/a), Adv. Sci. (2026) e22500, https://doi.org/10.1002/advs.202522500.
[11] K. Che, C. Yuan, H.J. Qi, J. Meaud, Viscoelastic multistable architected materials with temperature-dependent snapping sequence, Soft Matter 14 (13) (2018) 2492–2499, https://doi.org/10.1039/C8SM00217G.
[12] H. Niknam, A. Akbarzadeh, D. Therriault, S. Bodkhe, Tunable thermally bistable multi-material structure, Appl. Mater. Today 28 (2022) 101529, https://doi.org/10.1016/j.apmt.2022.101529.
[13] Q. Wang, B. Yang, R. Lin, L. He, Z. Liu, Temperature-regulated boundary constrain multistable structures and designed metamaterials, Smart Mater. Struct. 34 (9) (2025) 095041, https://doi.org/10.1088/1361-665X/ae0905.
[14] M. Pelliciari, F.O. Falope, L. Lanzoni, A.M. Tarantino, Theoretical and experimental analysis of the von Mises truss subjected to a horizontal load using a new hyperelastic model with hardening, Eur. J. Mech. - ASolids 97 (2023) 104825, https://doi.org/10.1016/j.euromechsol.2022.104825.
[15] M.N. Hasan, et al., Beyond von Mises truss models: emergent bistability in mechanical metamaterials, Phys. Rev. Appl. 25 (1) (Jan. 2026) 014029, https://doi.org/10.1103/yrnh-tbd8.

[16] Z. Meng, M. Liu, H. Yan, G.M. Genin, C.Q. Chen, Deployable mechanical metamaterials with multistep programmable transformation, Sci. Adv. 8 (23) (2022) eabn5460, https://doi.org/10.1126/sciadv.abn5460.
[17] S. Shan, et al., Multistable architected materials for trapping elastic strain energy, Adv. Mater. 27 (29) (2015) 4296–4301, https://doi.org/10.1002/adma.201501708.
[18] T.R. Giri, R. Mailen, Controlled snapping sequence and energy absorption in multistable mechanical metamaterial cylinders, Int. J. Mech. Sci. 204 (2021) 106541, https://doi.org/10.1016/j.ijmecsci.2021.106541.
[19] P.R. Kuppens, M.A. Bessa, J.L. Herder, J.B. Hopkins, Monolithic binary stiffness building blocks for mechanical digital machines, Extrem. Mech. Lett. 42 (2021) 101120, https://doi.org/10.1016/j.eml.2020.101120.
[20] H. Zhang, J. Wu, D. Fang, Y. Zhang, Hierarchical mechanical metamaterials built with scalable tristable elements for ternary logic operation and amplitude modulation, Sci. Adv. 7 (9) (2021) eabf1966, https://doi.org/10.1126/sciadv.abf1966.
[21] K. Liang, Y. Wang, Y. Luo, A. Takezawa, X. Zhang, Z. Kang, Programmable and multistable metamaterials made of precisely tailored bistable cells, Mater. Des. 227 (2023) 111810, https://doi.org/10.1016/j.matdes.2023.111810.
[22] T. Schioler, S. Pellegrino, Space frames with multiple stable configurations, AIAA J. 45 (7) (2007) 1740–1747, https://doi.org/10.2514/1.16825.
[23] S.A. Zirbel, K.A. Tolman, B.P. Trease, L.L. Howell, Bistable mechanisms for space applications, PLOS ONE 11 (12) (2016) e0168218, https://doi.org/10.1371/journal.pone.0168218.
[24] T. Chen, O.R. Bilal, K. Shea, C. Daraio, Harnessing bistability for directional propulsion of soft, untethered robots, Proc. Natl. Acad. Sci. USA 115 (22) (2018) 5698–5702, https://doi.org/10.1073/pnas.1800386115.
[25] B. Zhang, et al., Multistable soft robots assembled from bistable auxetic building blocks, Adv. Intell. Syst. 7 (4) (2025) 2400529, https://doi.org/10.1002/aisy.202400529.
[26] J.C. Osorio, J.S. Rincon, H. Morgan, A.F. Arrieta, Embodying control in soft multistable robots from morphofunctional co-design, Adv. Sci. 12 (32) (2025) e03206, https://doi.org/10.1002/advs.202503206.
[27] J. Qiu, J.H. Lang, A.H. Slocum, A curved-beam bistable mechanism, J. Micro Syst. 13 (2) (2004) 137–146, https://doi.org/10.1109/JMEMS.2004.825308.
[28] X. Tan, S. Chen, B. Wang, S. Zhu, L. Wu, Y. Sun, Design, fabrication, and characterization of multistable mechanical metamaterials for trapping energy, Extrem. Mech. Lett. 28 (2019) 8–21, https://doi.org/10.1016/j.eml.2019.02.002.
[29] D. Pan, Y. Xu, W. Li, Z. Wu, Novel rotational motion actuated beam-type multistable metastructures, Mater. Des. 224 (2022) 111309, https://doi.org/10.1016/j.matdes.2022.111309.
[30] D. Pan, S. Tan, Z. Zhang, W. Li, The metastructures actuated by rotational motion with quasi-zero stiffness, negative stiffness, and bistability, Thin-Walled Struct. 207 (2025) 112700, https://doi.org/10.1016/j.tws.2024.112700.
[31] P. Ducarme, B. Weber, M. van Hecke, J.T.B. Overvelde, Exotic mechanical properties enabled by countersnapping instabilities, Proc. Natl. Acad. Sci. USA 122 (16) (2025) e2423301122, https://doi.org/10.1073/pnas.2423301122.
[32] D. Pan, Z. Wu, F. Dai, N. Tolou, A novel design and manufacturing method for compliant bistable structure with dissipated energy feature, Mater. Des. 196 (2020) 109081, https://doi.org/10.1016/j.matdes.2020.109081.
[33] M. Hosseinabadi, E. Etemadi, A. Serjouei, M. Bodaghi, 3D printed negative stiffness meta-structures with superior energy absorption and super-elastic shape-recovery features, Smart Mater. Struct. (2023), https://doi.org/10.1088/1361-665X/acb6d9.
[34] E. Bronstein, D. Ilssar, V. Kannan, D.M. Kochmann, Silicon-based microscale multistable metamaterials: microfabrication and characterization, Exp. Mech. (Dec. 2025), https://doi.org/10.1007/s11340-025-01258-y.
[35] F. Pan, Y. Li, Z. Li, J. Yang, B. Liu, Y. Chen, 3D pixel mechanical metamaterials, Adv. Mater. 31 (25) (2019) 1900548, https://doi.org/10.1002/adma.201900548.
[36] H. Yang, L. Ma, Multi-stable mechanical metamaterials by elastic buckling instability, J. Mater. Sci. 54 (4) (2019) 3509–3526, https://doi.org/10.1007/s10853-018-3065-y.
[37] B. Zhang, Z. Meng, Y. Wang, 3D auxetic metamaterials with tunable multistable mechanical properties, Mech. Mater. 201 (2025) 105217, https://doi.org/10.1016/j.mechmat.2024.105217.
[38] T.E. Greenwood, et al., Soft multistable magnetic-responsive metamaterials, Sci. Adv. 11 (29) (2025) eadu3749, https://doi.org/10.1126/sciadv.adu3749.
[39] C. Cervi, S.T. Santillan, L.N. Virgin, Interrogating the Configuration Space of Postbuckled Beams, J. Eng. Mech. 149 (3) (2023) 04023009, https://doi.org/10.1061/JENMDT.EMENG-6839.
[40] S. Tan, D. Pan, Z. Wu, Multi-stable metastructure with multi-layer and multi-degree of freedom: a numerical and experimental investigation, Mater. Des. 240 (2024) 112859, https://doi.org/10.1016/j.matdes.2024.112859.
[41] Z. Wei, Y. Wu, H. Lai, J. Qian, Compression-twist coupling mechanical metamaterials with programmed bistability, Acta Mech. Solid. Sin. (2025) 1–9, https://doi.org/10.1007/s10338-025-00583-y.
[42] A.S. Meeussen, M. van Hecke, Multistable sheets with rewritable patterns for switchable shape-morphing, Nature 621 (7979) (2023) 516–520, https://doi.org/10.1038/s41586-023-06353-5.
[43] P. Roberjot, J.L. Herder, A unified design method for 2D auxetic metamaterials based on a minimal auxetic structure, Int. J. Solids Struct. 295 (2024) 112777, https://doi.org/10.1016/j.ijsolstr.2024.112777.
[44] P. Roberjot, J.L. Herder, A unified planar Poisson's ratio design method (PPRDM) for meiotic metamaterials that exhibit negative compressibility based on a minimal chiral meiotic structure, Int. J. Solids Struct. 320 (2025) 113494, https://doi.org/10.1016/j.ijsolstr.2025.113494.
[45] P. Roberjot, R. van den Bergh, J.L. Herder, A unified spatial Poisson's ratio design method (SPRDM) for 3D Poisson's ratio metamaterials based on a minimal chiral structure, Mater. Des. (2026) 115796, https://doi.org/10.1016/j.matdes.2026.115796.
[46] K. Wen, G. Wu, Design and analysis of a serial position-controlled variable stiffness rotating mechanism based on multi-stage torsional compliant mechanisms, Actuators 14 (5) (2025) 236, https://doi.org/10.3390/act14050236.
[47] T. van Noordt, J. t'Sas, N. Verzijl, L. Wong, J.L. Herder, P. Roberjot, A framework for the design of a magnet-based multistable rotational stage. Presented at the ASME 2025 International Design Engineering Technical Conferences and Computers and Information in Engineering Conference, American Society of Mechanical Engineers Digital Collection, Oct. 2025, https://doi.org/10.1115/DETC2025-167855.
[48] H.Y. Jeong, et al., 3D printing of twisting and rotational bistable structures with tuning elements, Sci. Rep. 9 (1) (2019) 324, https://doi.org/10.1038/s41598-018-36936-6.
[49] M. Vangbo, An analytical analysis of a compressed bistable buckled beam, Sens. Actuators Phys. 69 (3) (Sep. 1998) 212–216, https://doi.org/10.1016/S0924-4247(98)00097-1.
[50] P. Cazottes, A. Fernandes, J. Pouget, M. Hafez, Bistable buckled beam: modeling of actuating force and experimental validations, J. Mech. Des. 131 (101001) (2009), https://doi.org/10.1115/1.3179003.
[51] B. Camescasse, A. Fernandes, J. Pouget, Bistable buckled beam: elastica modeling and analysis of static actuation, Int. J. Solids Struct. 50 (19) (2013) 2881–2893, https://doi.org/10.1016/j.ijsolstr.2013.05.005.
[52] M.A.M. Siddiqui, H. Zhou, Synthesizing precompressed beams As bistable compliant mechanisms. Presented at the ASME 2017 International Mechanical Engineering Congress and Exposition, American Society of Mechanical Engineers Digital Collection, Jan. 2018, https://doi.org/10.1115/IMECE2017-70336.
[53] T. Liu, G. Hao, Design of deployable structures by using bistable compliant mechanisms, Micromachines 13 (5) (May 2022) 651, https://doi.org/10.3390/mi13050651.
[54] F. Albertini, M.G. Tarantino, L. Daniel, Mechanical behavior of embedded bistable dome shell with tunable energy barrier asymmetry, Int. J. Mech. Sci. 263 (2024) 108762, https://doi.org/10.1016/j.ijmecsci.2023.108762.
[55] I.Z. Pane, T. Asano, Investigation on bistability and fabrication of bistable prestressed curved beam, Jpn. J. Appl. Phys. 47 (6S) (2008) 5291, https://doi.org/10.1143/JJAP.47.5291.
[56] J. Hua, Y. Zhou, C.Q. Chen, Design and analysis of a tunable multistable mechanical metamaterial, Int. J. Mech. Sci. 272 (2024) 109170, https://doi.org/10.1016/j.ijmecsci.2024.109170.
[57] M. Koh, Y. Wang, K. Shea, T. Chen, Shape reconfiguring bistable structures using heat activated fibers, Eng. Struct. 295 (2023) 116792, https://doi.org/10.1016/j.engstruct.2023.116792.
[58] J.B. Hopkins, R.H. Lee, P. Sainaghi, Using binary-stiffness beams within mechanical neural-network metamaterials to learn, Smart Mater. Struct. 32 (3) (2023) 035015, https://doi.org/10.1088/1361-665X/acb519.
[59] M. Schenk, S.D. Guest, J.L. Herder, Zero stiffness tensegrity structures, Int. J. Solids Struct. 44 (20) (2007) 6569–6583, https://doi.org/10.1016/j.ijsolstr.2007.02.041.
[60] M. Schenk, S. Guest, On zero stiffness, Proc. Inst. Mech. Eng. Part. C. J. Mech. Eng. Sci. 228 (10) (2014) 1701–1714, https://doi.org/10.1177/0954406213511903.
[61] R. Mak, A. Amoozandeh Nobaveh, G. Radaelli, J.L. Herder, A curved compliant differential mechanism with neutral stability, J. Mech. Robot. 16 (011003) (2023), https://doi.org/10.1115/1.4056867.
[62] S. Kok, A.A. Nobaveh, G. Radaelli, Neutrally stable double-curved shells by inflection point propagation, J. Mech. Phys. Solids 171 (2023) 105133, https://doi.org/10.1016/j.jmps.2022.105133.
[63] Ü. Sönmez, C.C. Tutum, A compliant bistable mechanism design incorporating elastica buckling beam theory and pseudo-rigid-body model, J. Mech. Des. 130 (042304) (2008), https://doi.org/10.1115/1.2839009.
[64] T. Liu, G. Hao, J. Zhu, P. Kuresangsai, S. Abdelaziz, E. Wehrle, Modeling compliant bistable mechanisms: an energy method based on the high-order smooth curvature model, Int. J. Mech. Sci. 275 (2024) 109315, https://doi.org/10.1016/j.ijmecsci.2024.109315.
[65] G. Hao, A framework of designing compliant mechanisms with nonlinear stiffness characteristics, Microsyst. Technol. 24 (4) (2018) 1795–1802, https://doi.org/10.1007/s00542-017-3538-y.
[66] Y. Chi, Y. Li, Y. Zhao, Y. Hong, Y. Tang, J. Yin, Bistable and multistable actuators for soft robots: structures, materials, and functionalities, Adv. Mater. 34 (19) (2022) 2110384, https://doi.org/10.1002/adma.202110384.
[67] L.S. Novelino, Q. Ze, S. Wu, G.H. Paulino, R. Zhao, Untethered control of functional origami microrobots with distributed actuation, Proc. Natl. Acad. Sci. USA 117 (39) (2020) 24096–24101, https://doi.org/10.1073/pnas.2013292117.
[68] F. Liu, T. Terakawa, S. Long, M. Komori, Rigid-foldable cylindrical origami with tunable mechanical behaviors, Sci. Rep. 14 (1) (2024) 145, https://doi.org/10.1038/s41598-023-50353-4.
[69] S. Zang, T. Zhao, D. Misseroni, G.H. Paulino, Origami frustration and its influence on energy landscapes of origami assemblies, Proc. Natl. Acad. Sci. USA 122 (36) (2025) e2426790122, https://doi.org/10.1073/pnas.2426790122.
[70] T.A.M. Hewage, K.L. Alderson, A. Alderson, F. Scarpa, Double-negative mechanical metamaterials displaying simultaneous negative stiffness and

negative poisson's ratio properties, Adv. Mater. 28 (46) (2016) 10323–10332, https://doi.org/10.1002/adma.201603959.
[71] A. Rafsanjani, D. Pasini, Bistable auxetic mechanical metamaterials inspired by ancient geometric motifs, Extrem. Mech. Lett. 9 (2016) 291–296, https://doi.org/10.1016/j.eml.2016.09.001.
[72] T. Chen, J. Panetta, M. Schnaubelt, M. Pauly, Bistable auxetic surface structures, 1-39:9, juillet, ACM Trans. Graph. 40 (4) (2021) 39, https://doi.org/10.1145/3450626.3459940.
[73] Z. Meng, W. Chen, T. Mei, Y. Lai, Y. Li, C.Q. Chen, Bistability-based foldable origami mechanical logic gates, Extrem. Mech. Lett. 43 (2021) 101180, https://doi.org/10.1016/j.eml.2021.101180.
[74] Y. Yang, A. Vallecchi, E. Shamonina, C.J. Stevens, Z. You, A new class of transformable kirigami metamaterials for reconfigurable electromagnetic systems, Sci. Rep. 13 (1) (2023) 1219, https://doi.org/10.1038/s41598-022-27291-8.
[75] C. Qiao, F. Agnelli, D.K. Pokkalla, N. D'Ambrosio, D. Pasini, Anisotropic morphing in bistable kirigami through symmetry breaking and geometric frustration, Adv. Mater. 36 (23) (2024) 2313198, https://doi.org/10.1002/adma.202313198.
[76] N. Vasios, B. Deng, B. Gorissen, K. Bertoldi, Universally bistable shells with nonzero Gaussian curvature for two-way transition waves, Nat. Commun. 12 (1) (2021) 695, https://doi.org/10.1038/s41467-020-20698-9.
[77] C. Jiang, F. Rist, H. Wang, J. Wallner, H. Pottmann, Shape-morphing mechanical metamaterials, Comput. -Aided Des. 143 (2022) 103146, https://doi.org/10.1016/j.cad.2021.103146.
[78] L. Kong, Y.F. Zhao, From origami to bistable and laminate structures: a review for multifunctional applications from structural perspective of shape-changing structures (vol. n/a, no. n/a), Adv. Intell. Syst. (2025) 2500505, https://doi.org/10.1002/aisy.202500505.
[79] P. Zheng, B. Han, Z. Liu, Q. Wang, Z. Wang, Q. Zhang, Multistable twist metastructures with enhanced collapsibility and multidimensional programmability, Addit. Manuf. 95 (2024) 104550, https://doi.org/10.1016/j.addma.2024.104550.
[80] Y. Chi, Y. Li, Y. Zhao, Y. Hong, Y. Tang, J. Yin, Bistable and multistable actuators for soft robots: structures, materials, and functionalities, Adv. Mater. 34 (19) (2022) 2110384, https://doi.org/10.1002/adma.202110384.
[81] A.S. Meeussen, A. Corvi, K. Bertoldi, A new design strategy for highly multistable kirigami metamaterials, Adv. Funct. Mater. 35 (19) (2025) 2421638, https://doi.org/10.1002/adfm.202421638.
[82] E. Kebadze, S.D. Guest, S. Pellegrino, Bistable prestressed shell structures, Int. J. Solids Struct. 41 (11) (2004) 2801–2820, https://doi.org/10.1016/j.ijsolstr.2004.01.028.
[83] H.M.A. Kolken, A.A. Zadpoor, Auxetic mechanical metamaterials, RSC Adv. 7 (9) (2017) 5111–5129, https://doi.org/10.1039/C6RA27333E.
[84] M. Czajkowski, C. Coulais, M. van Hecke, D.Z. Rocklin, Conformal elasticity of mechanism-based metamaterials, Nat. Commun. 13 (1) (2022) 211, https://doi.org/10.1038/s41467-021-27825-0.
[85] K. Critchlow, Order in Space - Design Source Book, 1971. Accessed: Apr. 16, Thames and Hudson, 2025, http://archive.org/details/OrderInSpaceDesignSourceBookByKeithCritchlow, 1971. Accessed: Apr. 16.
[86] B. Grünbaum, Uniform tilings of 3-space, Geombinatorics 4 (2) (1994) 49–56.
[87] H.T. Pham, C.-T.P. Dang, N.T. Trung, V.T. Ngan, Transformation between hexagonal prism and antiprism of the singly and doubly cr-doped Ge12 clusters, J. Phys. Chem. A 123 (50) (2019) 10721–10729, https://doi.org/10.1021/acs.jpca.9b08052.
[88] Y. Zhang, Q. Wang, M. Tichem, F. van Keulen, Design and characterization of multi-stable mechanical metastructures with level and tilted stable configurations, Extrem. Mech. Lett. 34 (2020) 100593, https://doi.org/10.1016/j.eml.2019.100593.
[89] L. Lin, H. Zhang, C. Fan, The study on the properties of a metamaterial composed of star-shaped auxetic and curved-beam multi-stable structure, Mech. Adv. Mater. Struct. 31 (29) (2024) 11979–11995, https://doi.org/10.1080/15376494.2024.2313713.
[90] H. Yang, L. Ma, 1D to 3D multi-stable architected materials with zero Poisson's ratio and controllable thermal expansion, Mater. Des. 188 (2020) 108430, https://doi.org/10.1016/j.matdes.2019.108430.
[91] J.-J. Mao, S. Wang, W. Tan, M. Liu, Modular multistable metamaterials with reprogrammable mechanical properties, Eng. Struct. 272 (2022) 114976, https://doi.org/10.1016/j.engstruct.2022.114976.
[92] X. Ju, S. Li, Y. Zhang, P. Wu, Y. Li, Design of multi-stable metamaterial cell with improved and programmable energy trapping ability based on frame reinforced curved beams, Thin-Walled Struct. 202 (2024) 112120, https://doi.org/10.1016/j.tws.2024.112120.
[93] L. Li, B. Li, G. Chen, A non-transit fully compliant tristable mechanism capable of direct switching between every two stable positions, Mech. Syst. Signal. Process. 169 (2022) 108597, https://doi.org/10.1016/j.ymssp.2021.108597.
[94] B. Haghpanah, L. Salari-Sharif, P. Pourrajab, J. Hopkins, L. Valdevit, Multistable shape-reconfigurable architected materials, Adv. Mater. 28 (36) (2016) 7915–7920, https://doi.org/10.1002/adma.201601650.
[95] H. Liang, et al., The design of spatial compliant mechanisms with distributed multi-stability based on post-buckled cylindrical compliant beams, Mech. Syst. Signal. Process. 228 (2025) 112365, https://doi.org/10.1016/j.ymssp.2025.112365.
[96] R. Mak, A. Amoozandeh Nobaveh, G. Radaelli, J.L. Herder, A curved compliant differential mechanism with neutral stability, J. Mech. Robot. 16 (011003) (2023), https://doi.org/10.1115/1.4056867.
[97] A. Amoozandeh Nobaveh, J.L. Herder, G. Radaelli, Compliant variable negative to zero to positive stiffness twisting elements, Mech. Mach. Theory 196 (2024) 105607, https://doi.org/10.1016/j.mechmachtheory.2024.105607.
[98] R.M. Bichara, J. Costantine, Y. Tawk, M. Sakovsky, A multi-stable deployable quadrifilar helix antenna with radiation reconfigurability for disaster-prone areas, Nat. Commun. 14 (1) (2023) 8511, https://doi.org/10.1038/s41467-023-44189-9.
[99] T. Chen, K. Shea, Computational design of multi-stable, reconfigurable surfaces, Mater. Des. 205 (2021) 109688, https://doi.org/10.1016/j.matdes.2021.109688.
[100] C. Zhou, H. Qing, H. Sun, F. Qi, Y. Hong, J. Yin, Multistable thin-shell metastructures for multiresponsive reconfigurable metabots, Sci. Adv. 11 (42) (2025) eadx4359, https://doi.org/10.1126/sciadv.adx4359.
[101] H. Xiu, et al., Topological transformability and reprogrammability of multistable mechanical metamaterials, Proc. Natl. Acad. Sci. USA 119 (52) (2022) e2211725119, https://doi.org/10.1073/pnas.2211725119.
[102] T. Mei, Z. Meng, K. Zhao, C.Q. Chen, A mechanical metamaterial with reprogrammable logical functions, Nat. Commun. 12 (1) (2021) 7234, https://doi.org/10.1038/s41467-021-27608-7.
[103] G. Librandi, E. Tubaldi, K. Bertoldi, Programming nonreciprocity and reversibility in multistable mechanical metamaterials, Nat. Commun. 12 (1) (2021) 3454, https://doi.org/10.1038/s41467-021-23690-z.
[104] M.A. ten Wolde, D. Farhadi, A single-input state-switching building block harnessing internal instabilities, Mech. Mach. Theory 196 (2024) 105626, https://doi.org/10.1016/j.mechmachtheory.2024.105626.
[105] H.A. Johnson, et al., Signal propagation in reversible digital mechanics, Mater. Horiz. 12 (24) (2025) 10623–10629, https://doi.org/10.1039/D5MH00509D.
[106] Y. Song, et al., Additively manufacturable micro-mechanical logic gates, Nat. Commun. 10 (1) (2019) 882, https://doi.org/10.1038/s41467-019-08678-0.
[107] X. Hou, T. Sheng, F. Xie, Z. Deng, Mechanical logic gate design based on multi-stable metamaterial with multi-step deformation, Compos. Struct. 335 (2024) 118001, https://doi.org/10.1016/j.compstruct.2024.118001.